Robotica: (2020) volume 38, pp. 136–158. © Cambridge University Press 2019
doi:10.1017/S0263574719000523

Output Feedback Hybrid Force/Motion Control for Robotic Manipulators Interacting with Unknown Rigid Surfaces

Alejandro Gutiérrez–Giles†* and Marco Arteaga–Pérez‡

†*Department of Electrical Engineering and Information Technology, CREATE Consortium and Prisma Laboratory, University of Naples Federico II, Via Claudio 21, 80125 Naples, Italy*
‡*Departamento de Control y Robótica, DIE, Facultad de Ingeniería, Universidad Nacional Autónoma de México, Mexico City 04510, Mexico.*
E-mail: marteagp@unam.mx

(Accepted March 25, 2019. First published online: April 22, 2019)

SUMMARY
The problem of hybrid force and motion control over unknown rigid surfaces when only joint position measurements are available is considered. To overcome this problem, an extended state high-gain observer is designed to simultaneously estimate the contact force and joint velocities. These estimated signals are in turn employed to design a local estimator of the unknown surface gradient. This gradient is utilized to decompose the task space into two orthogonal subspaces: one for force tracking and the other one for motion control. A simple position Proportional Integral Derivative (PID) and force Proportional Integral (PI) controllers are proposed to track the desired signals. Finally, a mathematical analysis of the closed-loop dynamics is carried out, guaranteeing uniform ultimate boundedness of the position and force tracking errors and of the surface gradient estimation error. A numerical simulation is employed to validate the approach in an ideal scenario, while experiments are carried out to test the proposed strategy when uncertainties and unmodeled dynamics are present.

KEYWORDS: Force control; Observer design; Unknown environment; Ultimate boundedness.

1. Introduction

Many applications involving a robotic manipulator require its interaction with the environment. In such a case, it becomes necessary to control not only the motion of the manipulator but also the interaction force with the environment. There are basically two approaches to deal with the motion and force control problem: the direct and the indirect force control. To the latter category belong the so-called impedance and compliance controllers[1] that achieve the desired interaction force by controlling the motion of the manipulator without an explicit force control loop. These kinds of controllers are best suited for compliant environments (see, e.g., refs. [2–4]). On the other hand, direct force control comprehends the hybrid force/motion[5] and the parallel control.[6,7] The hybrid force/motion control is more suitable when the motion of the manipulator is restricted to a rigid surface (i.e., it can be represented by holonomic constraints), since it relies on the decomposition of the task space into motion-controlled and force-controlled subspaces.

For the mentioned approaches, it is commonly assumed that kinematic and dynamic models of both manipulator and environment are available. Moreover, it is assumed that positions, velocities, and contact force are measured. Several solutions have been proposed to deal with uncertainties on the surface geometry, including visual identification,[8–11] force-based reconstruction,[12] robustness against the kinematic and/or dynamic uncertainties,[13–15] and adaptive control.[16–21] In the case of

* Corresponding author. E-mail: giles.gutierrez@unina.it

compliant environments, the a priori exact description of the environment constraints is not always necessary, since the controllers can be designed to be robust against uncertainties in this description. In contrast, it has been shown that the geometric description of the constraints plays a critical role for the rigid surfaces case, since uncertainties in this description can easily lead to instability of the closed loop.[22]

The basic idea behind the mentioned schemes, when no exact description of the geometry of the constraints is available, is to reconstruct the surface by means of position, velocity, visual, and/or force measurements. Nevertheless, in many applications, it is desired to have the least number of sensors for a variety of reasons (reduction of weight, size, costs, etc.). Therefore, another interesting research direction is the output feedback motion and force control, that is, when only position measurements are available. Some solutions have been proposed to solve this problem for compliant surfaces, for example, an open-loop force control with adaptive identification of the surface,[23] extended active observers,[24] and sliding mode observers,[25] among others. For the rigid contact case, some solutions based on linear observers,[26,27] nonlinear PID observer-based control,[28] and generalized proportional integral observers[29] have been proposed as well.

On the other hand, the mentioned output feedback controllers over a rigid surface also need a precise description of the holonomic constrains, which is commonly obtained by means of kinematic calibration. However, there are some scenarios where this description cannot be obtained a priori, which represents an important disadvantage. Application examples of force control over an unknown environments that need the identification of the surface include exploration of unknown and dark spaces (tank, pipes, planets).[19] Regarding this problem, in ref. [30], a fault detection and isolation technique is employed to detect uncalibrated obstacles, and then a reconstruction of the contact force is utilized to regulate this force exerted over the unknown environment. The mentioned algorithm does not require force measurement nor acceleration but only joint positions and velocities.

In this work, an output feedback hybrid force/motion tracking controller for robotic manipulators subject to holonomic constraints with a local online estimation of the contact surface is proposed. The work is based on the Generalized Proportional Integral (GPI) observers methodology introduced in ref. [31] and further developed in ref. [29] to the case of contact force estimation. To the best of the authors' knowledge, there are no similar results for the problem treated here, that is, the hybrid force/motion control without force/velocity and/or vision measurements and without a geometric description of the surface. Although the main idea is similar to ref. [30], there are some differences and advantages in this work. The first difference is that, in contrast with ref. [30], no joint velocities are needed to implement the controller. A second distinction of our work is that the proposed surface gradient estimator is designed to be less sensitive to noise due to its filtering nature, which is an important practical advantage. Finally, in this work, a mathematical analysis is carried out, which gives conditions on the controller and observer parameters to guarantee the achieving of the control and estimation objective and the boundedness of all signals of interest.

The main contribution of this work is the design and implementation of a control algorithm that simultaneously estimates the joint velocities, the contact force, and the contact surface using only joint position measurements while following a desired trajectory both in position and in contact force. To the best of the authors' knowledge, this work is the first attempt to solve the problem presented here, that is, the closed-loop hybrid force/motion control over unknown surfaces using only joint position measurements.

The proposed approach guarantees ultimate boundedness of all the signals of interest, with arbitrarily small ultimate bounds, which means that force and position tracking, velocity and force reconstruction, and surface identification can be achieved with arbitrary precision in the ideal case. This is supported by the numerical simulations presented below. In a real scenario, this ultimate bound is no longer arbitrarily small due to several reasons, in particular to contact friction, which is assumed to be negligible for the control design and the stability analysis. Nevertheless, the experimental results presented below are in accordance with the expected performance.

This paper is organized as follows: in Section 2, a mathematical model of the system and some useful properties are presented. In Section 3, the main contribution of this work is developed, while in Section 4, both numerical simulations and experiments are shown to illustrate the effectiveness of the approach. Some concluding remarks and directions for future work are given in Section 5.

https://doi.org/10.1017/S0263574719000523 Published online by Cambridge University Press

2. Mathematical Model and Properties

Consider a n-degrees of freedom manipulator in contact with a rigid surface. Let $\boldsymbol{q} \in \mathbb{R}^n$ be the vector of generalized coordinates and $\boldsymbol{\tau} \in \mathbb{R}^n$ the vector of input torques. The corresponding dynamic model is given by[32]

$$\boldsymbol{H}(\boldsymbol{q})\ddot{\boldsymbol{q}} + \boldsymbol{C}(\boldsymbol{q}, \dot{\boldsymbol{q}})\dot{\boldsymbol{q}} + \boldsymbol{D}\dot{\boldsymbol{q}} + \boldsymbol{g}(\boldsymbol{q}) = \boldsymbol{\tau} + \boldsymbol{J}_{\varphi}^{\mathrm{T}}(\boldsymbol{q})\boldsymbol{\lambda}, \tag{1}$$

where $\boldsymbol{H}(\boldsymbol{q}) \in \mathbb{R}^{n\times n}$ is the inertia matrix, $\boldsymbol{C}(\boldsymbol{q}, \dot{\boldsymbol{q}})\dot{\boldsymbol{q}} \in \mathbb{R}^n$ is the vector of Coriolis and centripetal torques, $\boldsymbol{D} \in \mathbb{R}^{n\times n}$ is the diagonal matrix of viscous friction coefficients, $\boldsymbol{g}(\boldsymbol{q}) \in \mathbb{R}^n$ is the vector of gravity torques, $\boldsymbol{\lambda} \in \mathbb{R}^m$ is a vector of Lagrange multipliers (physically represents the force exerted by the manipulator over the environment at the contact point), and $\boldsymbol{J}_{\varphi}(\boldsymbol{q}) \triangleq \partial\boldsymbol{\varphi}(\boldsymbol{q})/\partial\boldsymbol{q} \in \mathbb{R}^{m\times n}$ is the gradient of the m holonomic constraints, specified in terms of the generalized coordinates, defined by

$$\boldsymbol{\varphi}(\boldsymbol{q}) = \boldsymbol{0}. \tag{2}$$

These constraints can also be defined in terms of the end effector coordinates $\boldsymbol{x} \in \mathbb{R}^n$, that is,

$$\boldsymbol{\varphi}(\boldsymbol{x}) = \boldsymbol{0}. \tag{3}$$

The gradient of this constraint $\boldsymbol{J}_{\varphi \mathrm{x}} \triangleq \partial\boldsymbol{\varphi}(\boldsymbol{x})/\partial\boldsymbol{x} \in \mathbb{R}^{m\times n}$ is related to $\boldsymbol{J}_{\varphi}(\boldsymbol{q})$ by

$$\boldsymbol{J}_{\varphi}(\boldsymbol{q}) = \boldsymbol{J}_{\varphi \mathrm{x}}\boldsymbol{J}(\boldsymbol{q}), \tag{4}$$

where $\boldsymbol{J}(\boldsymbol{q}) \in \mathbb{R}^{n\times n}$ is the analytic Jacobian of the manipulator. Note that with a suitable normalization, it can always be obtained $\|\boldsymbol{J}_{\varphi \mathrm{x}}\| = 1$. In this paper, it is assumed that this is the case. In addition, it is made the following rather standard assumption, which should be taken into account at the trajectory planning stage.

Assumption 2.1. *The manipulator never reaches a singularity, so* $\boldsymbol{J}^{-1}(\boldsymbol{q})$ *always exists* [1]. □

Some useful properties of the model (1) are listed. Notice that for the sake of simplicity, it is assumed that the robot has only revolute joints.

Property 2.1. *The inertia matrix* $\boldsymbol{H}(\boldsymbol{q})$ *is symmetric positive definite and* $\forall \boldsymbol{q}, \boldsymbol{y} \in \mathbb{R}^n$*; it holds* $\lambda_{\mathrm{h}}\|\boldsymbol{y}\|^2 \leq \boldsymbol{y}^{\mathrm{T}}\boldsymbol{H}(\boldsymbol{q})\boldsymbol{y} \leq \lambda_{\mathrm{H}}\|\boldsymbol{y}\|^2$*, with* $0 < \lambda_{\mathrm{h}} \leq \lambda_{\mathrm{H}} < \infty$. □

Property 2.2. *With a proper definition of* $\boldsymbol{C}(\boldsymbol{q}, \dot{\boldsymbol{q}})$*, the matrix* $\dot{\boldsymbol{H}}(\boldsymbol{q}) - 2\boldsymbol{C}(\boldsymbol{q}, \dot{\boldsymbol{q}})$ *is skew symmetric.* □

Property 2.3. *The vector* $\boldsymbol{C}(\boldsymbol{q}, \boldsymbol{x})\boldsymbol{y}$ *satisfies* $\boldsymbol{C}(\boldsymbol{q}, \boldsymbol{x})\boldsymbol{y} = \boldsymbol{C}(\boldsymbol{q}, \boldsymbol{y})\boldsymbol{x}$, $\forall \boldsymbol{x}, \boldsymbol{y} \in \mathbb{R}^n$. □

When the tip of the robot is in contact with a rigid surface, a local decomposition of the task space can be done as follows. Let $\boldsymbol{J}_{\varphi}^{+} = \boldsymbol{J}_{\varphi}^{\mathrm{T}}\left(\boldsymbol{J}_{\varphi}\boldsymbol{J}_{\varphi}^{\mathrm{T}}\right)^{-1} \in \mathbb{R}^{n\times m}$, $\boldsymbol{P}(\boldsymbol{q}) = \boldsymbol{J}_{\varphi}^{+}\boldsymbol{J}_{\varphi} \in \mathbb{R}^{n\times n}$, and $\boldsymbol{Q}(\boldsymbol{q}) = \boldsymbol{I}_{n\times n} - \boldsymbol{P}(\boldsymbol{q}) \in \mathbb{R}^{n\times n}$, whence $\boldsymbol{Q}$ and $\boldsymbol{P}$ are orthogonal projection matrices, that is, $\boldsymbol{QP} = \boldsymbol{O}$, $\boldsymbol{QJ}_{\varphi} = \boldsymbol{O}$, and $\boldsymbol{J}_{\varphi}^{\mathrm{T}}\boldsymbol{Q} = \boldsymbol{O}$. Furthermore, $\boldsymbol{QQ} = \boldsymbol{Q}$ and $\boldsymbol{PP} = \boldsymbol{P}$. Then, the following can be stated.

Property 2.4. *The vector* $\dot{\boldsymbol{q}}$ *can be written as*

$$\dot{\boldsymbol{q}} = \boldsymbol{Q}(\boldsymbol{q})\dot{\boldsymbol{q}} + \boldsymbol{P}(\boldsymbol{q})\dot{\boldsymbol{q}} = \boldsymbol{Q}(\boldsymbol{q})\dot{\boldsymbol{q}}. \tag{5}$$

□

Finally, an useful fact concerning the position tracking error vector and the subspaces projected by $\boldsymbol{Q}$ and $\boldsymbol{P}$ is stated. Let $\boldsymbol{q}_d \in \mathbb{R}^n$ be the desired position in articular coordinates, then the tracking error $\boldsymbol{e} \triangleq \boldsymbol{q} - \boldsymbol{q}_{\mathrm{d}}$ satisfies the following:[34]

Fact 2.1. *Assume* $\boldsymbol{q}_{\mathrm{d}}$ *is designed to satisfy* $\boldsymbol{\varphi}(\boldsymbol{q}_{\mathrm{d}}) = \boldsymbol{0}$*. Whenever the manipulator is restricted to fulfill the constraint (2) and the tracking error* $\boldsymbol{e}$ *is sufficiently small, the following approximation can be made:*

$$\boldsymbol{e} \approx \boldsymbol{Q}(\boldsymbol{q})\boldsymbol{e}, \tag{6}$$

[1] This condition should be checked at the robot initial configuration and at the trajectory generation stage, what can be done by computing the manipulability ellipsoids as shown in ref. [33, Sec. 3.9].

https://doi.org/10.1017/S0263574719000523 Published online by Cambridge University Press

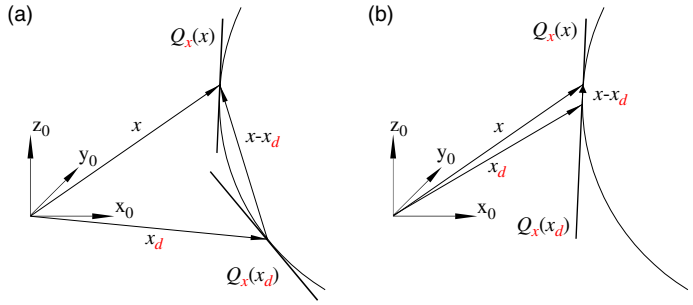

Fig. 1. Illustration of Fact 2.1: (a) error $\boldsymbol{e}$ not contained in the subspace projected by $\boldsymbol{Q}$ and (b) error $\boldsymbol{e}$ contained in the subspace projected by $\boldsymbol{Q}$.

because the error tends to be contained in the tangent subspace at the point $\boldsymbol{q}$ *projected by* $\boldsymbol{Q}(\boldsymbol{q})$. *Furthermore, from Property 2.4, it follows:*

$$\dot{\boldsymbol{q}}_{\mathrm{d}} \approx \boldsymbol{Q}(\boldsymbol{q})\dot{\boldsymbol{q}}_{\mathrm{d}} \Longrightarrow \dot{\boldsymbol{e}} \approx \boldsymbol{Q}(\boldsymbol{q})(\dot{\boldsymbol{q}} - \dot{\boldsymbol{q}}_{\mathrm{d}}) = \boldsymbol{Q}(\boldsymbol{q})\dot{\boldsymbol{e}}. \tag{7}$$

□

Remark 2.1. As illustrated in Figure 1 of ref. [34], which we reproduce here as Fig. 1, Fact 2.1 does not necessarily imply $\boldsymbol{e} \approx \boldsymbol{0}$. Roughly speaking, it says that the error is contained mostly in the subspace projected by $\boldsymbol{Q}(\boldsymbol{q})$ in a neighborhood of $\boldsymbol{e} = \boldsymbol{0}$. Furthermore, for a planar surface it is trivially satisfied. □

3. Main Result

Consider the case when the constraint is one dimensional (i.e., $m = 1$), so that $\boldsymbol{\lambda} = \lambda \in \mathbb{R}$ represents the scalar force that exerts the manipulator over the surface and $\boldsymbol{J}_{\varphi \mathrm{x}}$ maps every vector in the Cartesian space into the normal to the tangent plane to the surface at the contact point.

Let $\boldsymbol{q}_1 \triangleq \boldsymbol{q}$ and $\boldsymbol{q}_2 \triangleq \dot{\boldsymbol{q}}$. A state space representation of model (1) is given by

$$\dot{\boldsymbol{q}}_1 = \boldsymbol{q}_2, \tag{8}$$

$$\dot{\boldsymbol{q}}_2 = \boldsymbol{H}^{-1}(\boldsymbol{q}_1)\left(\boldsymbol{\tau} - \boldsymbol{N}(\boldsymbol{q}_1, \boldsymbol{q}_2)\right) + \boldsymbol{z}_1, \tag{9}$$

where $\boldsymbol{N}(\boldsymbol{q}_1, \boldsymbol{q}_2) \triangleq \boldsymbol{C}(\boldsymbol{q}_1, \boldsymbol{q}_2)\boldsymbol{q}_2 + \boldsymbol{D}\boldsymbol{q}_2 + \boldsymbol{g}(\boldsymbol{q}_1)$ and

$$\boldsymbol{z}_1 \triangleq \boldsymbol{H}^{-1}(\boldsymbol{q}_1)\boldsymbol{J}_{\varphi}^{\mathrm{T}}(\boldsymbol{q}_1)\lambda. \tag{10}$$

One of the goals of this work is to estimate the contact force λ, contained in the variable $\boldsymbol{z}_1$. We make the following assumptions concerning $\boldsymbol{z}_1$:[31]

Assumption 3.1. *The vector* $\boldsymbol{z}_1$ *can be locally modeled as a vector of Taylor polynomials in the time variable* t, *plus a residual term, that is,*

$$\boldsymbol{z}_1(t) = \sum_{i=1}^{p} \boldsymbol{a}_i t^i + \boldsymbol{r}(t), \tag{11}$$

where $\boldsymbol{a}_i \in \mathbb{R}^n, i = 1, \ldots, p$ *are vectors of constant coefficients and* $\boldsymbol{r}(t) \in \mathbb{R}^n$ *is the residual term.* □

Assumption 3.2. *At least the first* p *time derivatives of* $\boldsymbol{z}_1$ *exist.* □

Assumptions 3.1 and 3.2 allow us to write an internal model of $\boldsymbol{z}_1$ for the foregoing estimation as

$$\dot{\boldsymbol{z}}_1 = \boldsymbol{z}_2 \tag{12}$$

$$\dot{\boldsymbol{z}}_2 = \boldsymbol{z}_3 \tag{13}$$

$$\vdots$$

https://doi.org/10.1017/S0263574719000523 Published online by Cambridge University Press

$$\dot{z}_{p-1} = z_p \tag{14}$$

$$\dot{z}_p = \boldsymbol{r}^{(p)}(t). \tag{15}$$

Taking into account this model, the extended state observer is proposed:[31]

$$\dot{\hat{\boldsymbol{q}}}_1 = \hat{\boldsymbol{q}}_2 + \boldsymbol{\lambda}_{p+1}\tilde{\boldsymbol{q}}_1 \tag{16}$$

$$\dot{\hat{\boldsymbol{q}}}_2 = \boldsymbol{H}^{-1}(\boldsymbol{q}_1)\left(\boldsymbol{\tau} - \boldsymbol{N}(\boldsymbol{q}_1, \hat{\boldsymbol{q}}_2)\right) + \hat{z}_1 + \boldsymbol{\lambda}_p\tilde{\boldsymbol{q}}_1 \tag{17}$$

$$\dot{\hat{z}}_1 = \hat{z}_2 + \boldsymbol{\lambda}_{p-1}\tilde{\boldsymbol{q}}_1 \tag{18}$$

$$\dot{\hat{z}}_2 = \hat{z}_3 + \boldsymbol{\lambda}_{p-2}\tilde{\boldsymbol{q}}_1 \tag{19}$$

$$\vdots$$

$$\dot{\hat{z}}_{p-1} = \hat{z}_p + \boldsymbol{\lambda}_1\tilde{\boldsymbol{q}}_1 \tag{20}$$

$$\dot{\hat{z}}_p = \boldsymbol{\lambda}_0\tilde{\boldsymbol{q}}_1, \tag{21}$$

where $\tilde{\boldsymbol{q}}_1 \triangleq \boldsymbol{q}_1 - \hat{\boldsymbol{q}}_1$ and $\boldsymbol{N}(\boldsymbol{q}_1, \hat{\boldsymbol{q}}_2) \triangleq \boldsymbol{C}(\boldsymbol{q}_1, \hat{\boldsymbol{q}}_2)\hat{\boldsymbol{q}}_2 + \boldsymbol{D}\hat{\boldsymbol{q}}_2 + \boldsymbol{g}(\boldsymbol{q}_1)$. Note that $\hat{\boldsymbol{q}}_2$ is employed instead of $\boldsymbol{q}_2$ to avoid velocity measurements.

From Eqs. (4) and (10) it follows:

$$\boldsymbol{J}_{\varphi x}^{\mathrm{T}}\lambda = \boldsymbol{J}^{-\mathrm{T}}(\boldsymbol{q}_1)\boldsymbol{H}(\boldsymbol{q}_1)z_1. \tag{22}$$

As mentioned above, the Lagrange multiplier λ represents the contact force and $\|\boldsymbol{J}_{\varphi x}^{\mathrm{T}}\|$ is a unitary vector in the normal direction to the surface. For unidirectional constraints, it is $\lambda \geq 0$. By taking the Euclidean norm in both sides of Eq. (22), an estimate of the contact force can be obtained by

$$\hat{\lambda} = \|\boldsymbol{J}_{\varphi x}^{\mathrm{T}}\hat{\boldsymbol{\lambda}}\| = \|\boldsymbol{J}^{-\mathrm{T}}(\boldsymbol{q}_1)\boldsymbol{H}(\boldsymbol{q}_1)\hat{z}_1\|. \tag{23}$$

Because it is assumed that the geometry of the constraint surface is unknown, an online estimation of the gradient of this surface in workspace coordinates is proposed as

$$\dot{\hat{\boldsymbol{J}}}_{\varphi x}^{\mathrm{T}} = \left(\frac{\gamma}{\hat{\lambda} + \epsilon}\right)\hat{\boldsymbol{Q}}_x\boldsymbol{J}^{-\mathrm{T}}(\boldsymbol{q}_1)\boldsymbol{H}(\boldsymbol{q}_1)\hat{z}_1, \tag{24}$$

where $\gamma > 0$ is a scalar adaptation gain, $\epsilon << \lambda$ is a (small) positive constant to avoid division by zero, and $\hat{\boldsymbol{Q}}_x \triangleq \boldsymbol{I} - \hat{\boldsymbol{J}}_{\varphi x}^{\mathrm{T}}\left(\hat{\boldsymbol{J}}_{\varphi x}\hat{\boldsymbol{J}}_{\varphi x}^{\mathrm{T}}\right)^{-1}\hat{\boldsymbol{J}}_{\varphi x}$. Since from the definition of $\hat{\boldsymbol{Q}}_{\varphi x}$, $\hat{\boldsymbol{J}}_{\varphi x}\hat{\boldsymbol{Q}}_x = \boldsymbol{0}$; after Eq. (24) it is

$$\frac{\mathrm{d}}{\mathrm{d}t}\left(\|\hat{\boldsymbol{J}}_{\varphi x}\|^2\right) = \frac{\mathrm{d}}{\mathrm{d}t}\left(\hat{\boldsymbol{J}}_{\varphi x}\hat{\boldsymbol{J}}_{\varphi x}^{\mathrm{T}}\right) = 2\hat{\boldsymbol{J}}_{\varphi x}\dot{\hat{\boldsymbol{J}}}_{\varphi x}^{\mathrm{T}} = \left(\frac{2\gamma}{\hat{\lambda} + \epsilon}\right)\hat{\boldsymbol{J}}_{\varphi x}\hat{\boldsymbol{Q}}_x\boldsymbol{J}^{-\mathrm{T}}(\boldsymbol{q}_1)\boldsymbol{H}(\boldsymbol{q}_1)\hat{z}_1 = \boldsymbol{0}. \tag{25}$$

Then, $\|\hat{\boldsymbol{J}}_{\varphi x}\| \equiv 1$ as long as $\|\hat{\boldsymbol{J}}_{\varphi x}(t_0)\| = 1$, which is assumed in this work. Hence, the computation of $\hat{\boldsymbol{Q}}_x$ is simplified to

$$\hat{\boldsymbol{Q}}_x = \boldsymbol{I} - \hat{\boldsymbol{J}}_{\varphi x}^{\mathrm{T}}\hat{\boldsymbol{J}}_{\varphi x}. \tag{26}$$

Additionally, it is defined $\hat{\boldsymbol{P}}_x \triangleq \boldsymbol{I} - \hat{\boldsymbol{Q}}_x$.

Remark 3.1. Without the term $\hat{\boldsymbol{Q}}_x$, the gradient estimator is just a filtered version of the estimated force vector divided by its module. This idea has been employed in the literature when force measurement is available.[16,20,21] The introduction of $\hat{\boldsymbol{Q}}_x$ is proposed to ensure the norm invariance of $\hat{\boldsymbol{J}}_{\varphi x}$ as shown in Eq. (25). □

When dealing with position control over uncertain surfaces, one major issue is trajectory planning. Although the geometry of the environment is considered to be unknown, we make the following assumption to simplify the problem.

https://doi.org/10.1017/S0263574719000523 Published online by Cambridge University Press

Assumption 3.3. *The unknown contact surface is smooth, that is, it can be described by a continuous function (3) with continuous derivatives of all orders with respect to the Cartesian coordinates* $\boldsymbol{x}$. □

We also assume that the tip of the robot is in contact with this surface at $t = t_0$.

Remark 3.2. Although there is no restriction on the concavity, convexity, or maximum/minimum gradient of the surface, in a practical application, it can be limited by the geometry of the manipulator tip. To deal with the problem of the tip being in contact with the unknown surface at $t = t_0$ without force sensor, the very same force estimator (23) can be employed in free movement to detect a collision, after some predefined threshold (as in ref.[30]). □

This way, a locally linear approximation is developed to solve the trajectory planning problem (see ref. [21] for details). Let $\eta > 0$ and let $\boldsymbol{x}_a \in \mathbb{R}^n$ be the output of the unit-gain first-order filter

$$\dot{\boldsymbol{x}}_{\mathrm{a}} = -\eta \boldsymbol{x}_{\mathrm{a}} + \eta \boldsymbol{x}, \tag{27}$$

with $\boldsymbol{x}_{\mathrm{a}}(t_0)$ the robot tip position at the beginning of the task. For low frequencies, this is equivalent to computing a delayed version of $\boldsymbol{x}$, that is, $\boldsymbol{x}_{\mathrm{a}} \approx \boldsymbol{x}(t - T)$ for some $T > 0$.

The desired position in Cartesian coordinates $\boldsymbol{x}_{\mathrm{d}}(t) \in \mathbb{R}^n$ can then be computed online to fulfill

$$\hat{\boldsymbol{\varphi}}(\boldsymbol{x}) = \hat{\boldsymbol{J}}_{\varphi \mathrm{x}}(\boldsymbol{x}_{\mathrm{d}}(t) - \boldsymbol{x}_{\mathrm{a}}) = \boldsymbol{0}. \tag{28}$$

The corresponding desired position in joint coordinates $\boldsymbol{q}_{\mathrm{d}} \in \mathbb{R}^n$ is obtained by solving the inverse kinematics of the manipulator. Finally, let $\lambda_{\mathrm{d}} = \lambda_{\mathrm{d}}(t) \in \mathbb{R}$ be the desired contact force; then the observer-based hybrid position/force control is proposed:

$$\boldsymbol{\tau} = -\boldsymbol{K}_{\mathrm{p}} \boldsymbol{e}_1 - \boldsymbol{K}_{\mathrm{v}}(\hat{\boldsymbol{q}}_2 - \dot{\boldsymbol{q}}_{\mathrm{d}}) - \hat{\boldsymbol{Q}} \boldsymbol{K}_{\mathrm{i}} \int_0^t \boldsymbol{e}_1 \, \mathrm{d}\vartheta - \hat{\boldsymbol{J}}_{\varphi}^{\mathrm{T}} \lambda_{\mathrm{d}} + \hat{\boldsymbol{J}}_{\varphi}^{+} k_{\mathrm{Fi}} \Delta \bar{F}, \tag{29}$$

where $\boldsymbol{K}_{\mathrm{p}}, \boldsymbol{K}_{\mathrm{v}}, \boldsymbol{K}_{\mathrm{i}} \in \mathbb{R}^{n \times n}$ are diagonal positive definite matrices of constant gains, $k_{\mathrm{Fi}} > 0$ is the integral force control gain, $\boldsymbol{e}_1 \triangleq \boldsymbol{q}_1 - \boldsymbol{q}_{\mathrm{d}}$ is the position tracking error, and

$$\hat{\boldsymbol{J}}_{\varphi}^{\mathrm{T}} \triangleq \boldsymbol{J}(\boldsymbol{q}) \hat{\boldsymbol{J}}_{\varphi \mathrm{x}}^{\mathrm{T}}, \tag{30}$$

$$\hat{\boldsymbol{J}}_{\varphi}^{+} \triangleq \hat{\boldsymbol{J}}_{\varphi}^{\mathrm{T}} \left(\hat{\boldsymbol{J}}_{\varphi} \hat{\boldsymbol{J}}_{\varphi}^{\mathrm{T}} \right)^{-1}, \tag{31}$$

$$\hat{\boldsymbol{Q}} \triangleq \boldsymbol{I} - \hat{\boldsymbol{J}}_{\varphi}^{+} \hat{\boldsymbol{J}}_{\varphi}. \tag{32}$$

Additionally, it is defined:

$$\Delta \bar{\lambda} \triangleq \hat{\lambda} - \lambda_{\mathrm{d}}, \tag{33}$$

$$\Delta \bar{F} \triangleq \int_0^t \Delta \bar{\lambda} \, \mathrm{d}\vartheta. \tag{34}$$

Remark 3.3. The proposed observer (16)–(21) requires the dynamic model of the robot to estimate the term $\boldsymbol{z}_1$. Consequently, any modeling error or external disturbance will affect the contact force and the surface gradient estimation given by Eqs. (23) and (24), respectively. Additionally, it is assumed that contact friction can be neglected in the mathematical model (1). This assumption might be stringent, but it is not unrealistic for some scenarios (see ref. [19]). If contact friction cannot be neglected, then it should be explicitly included both in the model (1) and in the observer (16)–(21) similarly as proposed in ref. [35]. This high dependency on the model accuracy is a disadvantage that most force observers reported in the literature share, to the best of the authors' knowledge. In Section 4, we provide some experimental results to show that despite this disadvantage, our scheme was able to carry out the desired task. □

https://doi.org/10.1017/S0263574719000523 Published online by Cambridge University Press

3.1. Closed-loop dynamics

Let $\tilde{\boldsymbol{q}}_2 \triangleq \boldsymbol{q}_2 - \hat{\boldsymbol{q}}_2$ and $\tilde{z}_i \triangleq z_i - \hat{z}_i$, $i = 1, \ldots, p$. The dynamics of the state space model (8)–(9) and (12)–(15) in closed loop with the proposed observer (16)–(21) is given by

$$\dot{\tilde{\boldsymbol{q}}}_1 = \tilde{\boldsymbol{q}}_2 - \boldsymbol{\lambda}_{p+1}\tilde{\boldsymbol{q}}_1 \tag{35}$$

$$\dot{\tilde{\boldsymbol{q}}}_2 = -\boldsymbol{H}^{-1}(\boldsymbol{q}_1)\left(\boldsymbol{N}(\boldsymbol{q}_1, \boldsymbol{q}_2) - \boldsymbol{N}(\boldsymbol{q}_1, \hat{\boldsymbol{q}}_2)\right) + \tilde{z}_1 - \boldsymbol{\lambda}_p\tilde{\boldsymbol{q}}_1 \tag{36}$$

$$\dot{\tilde{z}}_1 = \tilde{z}_2 - \boldsymbol{\lambda}_{p-1}\tilde{\boldsymbol{q}}_1 \tag{37}$$

$$\dot{\tilde{z}}_2 = \tilde{z}_3 - \boldsymbol{\lambda}_{p-2}\tilde{\boldsymbol{q}}_1 \tag{38}$$

$$\vdots$$

$$\dot{\tilde{z}}_{p-1} = \tilde{z}_p - \boldsymbol{\lambda}_1\tilde{\boldsymbol{q}}_1 \tag{39}$$

$$\dot{\tilde{z}}_p = \boldsymbol{r}^{(p)}(t) - \boldsymbol{\lambda}_0\tilde{\boldsymbol{q}}_1. \tag{40}$$

By the same arguments as given in ref. [29], one can obtain

$$\ddot{\tilde{\boldsymbol{q}}}_1 + \boldsymbol{\lambda}_{p+1}\dot{\tilde{\boldsymbol{q}}}_1 + \boldsymbol{\lambda}_p\tilde{\boldsymbol{q}}_1 = \tilde{z}_1 + \boldsymbol{f}(t), \tag{41}$$

where

$$\boldsymbol{f}(t) \triangleq -\boldsymbol{H}^{-1}(\boldsymbol{q}_1)\Big[2\boldsymbol{C}\big(\boldsymbol{q}_1, \dot{\boldsymbol{e}}_1 + \dot{\boldsymbol{q}}_{\mathrm{d}}\big)\big(\dot{\tilde{\boldsymbol{q}}}_1 + \boldsymbol{\lambda}_{p+1}\tilde{\boldsymbol{q}}_1\big) - \boldsymbol{C}(\boldsymbol{q}_1, \dot{\tilde{\boldsymbol{q}}}_1 + \boldsymbol{\lambda}_{p+1}\tilde{\boldsymbol{q}}_1)\big(\dot{\tilde{\boldsymbol{q}}}_1 + \boldsymbol{\lambda}_{p+1}\tilde{\boldsymbol{q}}_1\big) + \boldsymbol{D}(\dot{\tilde{\boldsymbol{q}}}_1 + \boldsymbol{\lambda}_{p+1}\tilde{\boldsymbol{q}}_1)\Big]. \tag{42}$$

From Eqs. (37) to (40), it is easy to get

$$\tilde{z}_1^{(p)} = \boldsymbol{r}^{(p)}(t) - \boldsymbol{\lambda}_0\tilde{\boldsymbol{q}}_1 - \cdots - \boldsymbol{\lambda}_{p-1}\tilde{\boldsymbol{q}}_1^{(p-1)}. \tag{43}$$

Differentiating p-times (41) and using (43), one obtains

$$\tilde{\boldsymbol{q}}_1^{(p+2)} + \boldsymbol{\lambda}_{p+1}\tilde{\boldsymbol{q}}_1^{(p+1)} + \cdots + \boldsymbol{\lambda}_0\tilde{\boldsymbol{q}}_1 = \boldsymbol{r}^{(p)}(t) + \boldsymbol{f}^{(p)}(t). \tag{44}$$

Eq. (44) can be rewritten in a compact form as

$$\dot{\boldsymbol{x}}_{\mathrm{o}} = \boldsymbol{A}\boldsymbol{x}_{\mathrm{o}} + \boldsymbol{B}\boldsymbol{r}_{\mathrm{f}}, \tag{45}$$

where $\boldsymbol{r}_{\mathrm{f}} = \boldsymbol{r}^{(p)}(t) + \boldsymbol{f}^{(p)}(t)$ and

$$\boldsymbol{x}_{\mathrm{o}} \triangleq \begin{bmatrix} \tilde{\boldsymbol{q}}_1 & \cdots & \tilde{\boldsymbol{q}}_1^{(p+1)} \end{bmatrix}^{\mathrm{T}} \tag{46}$$

$$\boldsymbol{A} = \begin{bmatrix} \boldsymbol{O} & \boldsymbol{I} & \cdots & \boldsymbol{O} \\ \vdots & \vdots & \ddots & \vdots \\ \boldsymbol{O} & \boldsymbol{O} & \cdots & \boldsymbol{I} \\ -\boldsymbol{\lambda}_0 & -\boldsymbol{\lambda}_1 & \cdots & -\boldsymbol{\lambda}_{p+1} \end{bmatrix} \tag{47}$$

$$\boldsymbol{B} = \begin{bmatrix} \boldsymbol{O} & \cdots & \boldsymbol{O} & \boldsymbol{I} \end{bmatrix}^{\mathrm{T}}. \tag{48}$$

Consider for the sake of simplicity, $\boldsymbol{K}_{\mathrm{i}} = k_{\mathrm{i}}\boldsymbol{I}$. In order to carry out the stability analysis, the control law (29) is rewritten as

$$\boldsymbol{\tau} = -\boldsymbol{K}_{\mathrm{p}}\boldsymbol{e}_1 - \boldsymbol{K}_{\mathrm{v}}\dot{\boldsymbol{e}}_1 - \boldsymbol{K}_{\mathrm{i}}\boldsymbol{Q}\int_0^t \boldsymbol{e}_1\,\mathrm{d}\vartheta - \boldsymbol{J}_{\varphi}^{\mathrm{T}}\lambda_{\mathrm{d}} + k_{\mathrm{Fi}}\boldsymbol{J}_{\varphi}^{+}\Delta\bar{F} + \boldsymbol{K}_{\mathrm{v}}\big(\dot{\tilde{\boldsymbol{q}}}_1 + \boldsymbol{\lambda}_{p+1}\tilde{\boldsymbol{q}}_1\big) + \boldsymbol{K}_{\mathrm{i}}\tilde{\boldsymbol{Q}}\int_0^t \boldsymbol{e}_1\,\mathrm{d}\vartheta + \tilde{\boldsymbol{J}}_{\varphi}^{\mathrm{T}}\lambda_{\mathrm{d}} - k_{\mathrm{Fi}}\bar{\boldsymbol{J}}_{\varphi}^{+}\Delta\bar{F}, \tag{49}$$

https://doi.org/10.1017/S0263574719000523 Published online by Cambridge University Press

where $\tilde{\boldsymbol{Q}} \triangleq \boldsymbol{Q} - \hat{\boldsymbol{Q}}$, $\tilde{\boldsymbol{J}}_\varphi \triangleq \boldsymbol{J}_\varphi - \hat{\boldsymbol{J}}_\varphi$, and $\bar{\boldsymbol{J}}_\varphi^+ \triangleq \boldsymbol{J}_\varphi^+ - \hat{\boldsymbol{J}}_\varphi^+$. Next, it is defined

$$\dot{\boldsymbol{\sigma}} \triangleq \dot{\boldsymbol{e}}_1 + \boldsymbol{\Lambda}\boldsymbol{e}_1, \tag{50}$$

where $\boldsymbol{\Lambda} \in \mathbb{R}^{n\times n}$ is a diagonal positive definite gain matrix. Suppose that $\boldsymbol{Q}\boldsymbol{\Lambda} = \boldsymbol{\Lambda}\boldsymbol{Q}$ is satisfied, what can be accomplished just by setting

$$\boldsymbol{\Lambda} = k_\lambda \boldsymbol{I}, \tag{51}$$

with $k_\lambda > 0$. Now it is assumed momentarily that both $\boldsymbol{e}_1$ and $\dot{\boldsymbol{e}}_1$ satisfy Fact 2.1, so that it is possible to find $\bar{\boldsymbol{K}}_\mathrm{i} \in \mathbb{R}^{n\times n}$ such that

$$\boldsymbol{K}_\mathrm{p} = \boldsymbol{K}_\mathrm{v}\boldsymbol{\Lambda} + \bar{\boldsymbol{K}}_\mathrm{i}, \tag{52}$$

$$\boldsymbol{K}_\mathrm{i} = \bar{\boldsymbol{K}}_\mathrm{i}\boldsymbol{\Lambda}. \tag{53}$$

Hence, the control law (49) is equivalent to

$$\begin{aligned}\boldsymbol{\tau} = &-\boldsymbol{K}_\mathrm{v}\dot{\boldsymbol{\sigma}} - \bar{\boldsymbol{K}}_\mathrm{i}\boldsymbol{Q}\boldsymbol{\sigma} - \boldsymbol{J}_\varphi^\mathrm{T}\lambda_\mathrm{d} + k_\mathrm{Fi}\boldsymbol{J}_\varphi^+\Delta\bar{F} + \boldsymbol{K}_\mathrm{v}\big(\dot{\tilde{\boldsymbol{q}}}_1 + \boldsymbol{\lambda}_{p+1}\tilde{\boldsymbol{q}}_1\big)\\ &+ \boldsymbol{K}_\mathrm{i}\tilde{\boldsymbol{Q}}\int_0^t \boldsymbol{e}_1\,\mathrm{d}\vartheta + \tilde{\boldsymbol{J}}_\varphi^\mathrm{T}\lambda_\mathrm{d} - k_\mathrm{Fi}\bar{\boldsymbol{J}}_\varphi^+\Delta\bar{F}.\end{aligned} \tag{54}$$

Furthermore, it is defined

$$\dot{\boldsymbol{q}}_\mathrm{r} \triangleq \dot{\boldsymbol{q}}_\mathrm{d} - \boldsymbol{\Lambda}\boldsymbol{e}_1 - \boldsymbol{K}_\mathrm{v}^{-1}\bar{\boldsymbol{K}}_\mathrm{i}\boldsymbol{Q}\boldsymbol{\sigma} + \frac{1}{2}\boldsymbol{K}_\mathrm{v}^{-1}\boldsymbol{J}_\varphi^\mathrm{T}\Delta\lambda + \frac{1}{2}k_\mathrm{Fi}\boldsymbol{K}_\mathrm{v}^{-1}\boldsymbol{J}_\varphi^+\Delta\bar{F}, \tag{55}$$

$$\begin{aligned}\boldsymbol{s} &\triangleq \dot{\boldsymbol{q}} - \dot{\boldsymbol{q}}_\mathrm{r} = \big(\dot{\boldsymbol{\sigma}} + \boldsymbol{K}_\mathrm{v}^{-1}\bar{\boldsymbol{K}}_\mathrm{i}\boldsymbol{Q}\boldsymbol{\sigma}\big) + \left(-\frac{1}{2}\boldsymbol{K}_\mathrm{v}^{-1}\boldsymbol{J}_\varphi^\mathrm{T}\Delta\lambda - \frac{1}{2}k_\mathrm{Fi}\boldsymbol{K}_\mathrm{v}^{-1}\boldsymbol{J}_\varphi^+\Delta\bar{F}\right)\\ &\triangleq \boldsymbol{s}_\mathrm{p} + \boldsymbol{s}_\mathrm{F},\end{aligned} \tag{56}$$

where $\Delta\lambda \triangleq \lambda - \lambda_\mathrm{d}$ is the force tracking error. The closed-loop dynamics (omitting the arguments for simplicity) is given by

$$\boldsymbol{H}\dot{\boldsymbol{s}} + \boldsymbol{C}\boldsymbol{s} + \boldsymbol{K}_\mathrm{Dv}\boldsymbol{s} = \frac{1}{2}\boldsymbol{J}_\varphi^\mathrm{T}\Delta\lambda + \frac{1}{2}k_\mathrm{Fi}\boldsymbol{J}_\varphi^+\Delta\bar{F} + \boldsymbol{y}_\mathrm{a}, \tag{57}$$

where $\boldsymbol{K}_\mathrm{Dv} \triangleq \boldsymbol{K}_\mathrm{v} + \boldsymbol{D}$ and

$$\begin{aligned}\boldsymbol{y}_\mathrm{a} = &\boldsymbol{K}_\mathrm{v}(\dot{\tilde{\boldsymbol{q}}}_1 + \boldsymbol{\lambda}_{p+1}\tilde{\boldsymbol{q}}_1) + \boldsymbol{K}_\mathrm{i}\tilde{\boldsymbol{Q}}\int_0^t \boldsymbol{e}_1\,\mathrm{d}\vartheta + \tilde{\boldsymbol{J}}_\varphi^\mathrm{T}\lambda_\mathrm{d} - k_\mathrm{Fi}\tilde{\boldsymbol{J}}_\varphi^+\Delta\bar{F}\\ &- \big(\boldsymbol{H}(\boldsymbol{q})\ddot{\boldsymbol{q}}_\mathrm{r} + \boldsymbol{C}(\boldsymbol{q}_1, \boldsymbol{q}_2)\dot{\boldsymbol{q}}_\mathrm{r} + \boldsymbol{D}\dot{\boldsymbol{q}}_\mathrm{r} + \boldsymbol{g}(\boldsymbol{q})\big).\end{aligned} \tag{58}$$

Let $\tilde{\boldsymbol{J}}_{\varphi\mathrm{x}} \triangleq \boldsymbol{J}_{\varphi\mathrm{x}} - \hat{\boldsymbol{J}}_{\varphi\mathrm{x}}$ be the estimation error of the normal vector to the surface. By taking into account (24) it follows:

$$\dot{\tilde{\boldsymbol{J}}}_{\varphi\mathrm{x}}^\mathrm{T} = \dot{\boldsymbol{J}}_{\varphi\mathrm{x}}^\mathrm{T} - \dot{\hat{\boldsymbol{J}}}_{\varphi\mathrm{x}}^\mathrm{T} = \dot{\boldsymbol{J}}_{\varphi\mathrm{x}}^\mathrm{T} - \left(\frac{\gamma}{\hat{\lambda} + \epsilon}\right)\hat{\boldsymbol{Q}}_\mathrm{x}\boldsymbol{J}^{-\mathrm{T}}(\boldsymbol{q}_1)\boldsymbol{H}(\boldsymbol{q}_1)\hat{\boldsymbol{z}}_1. \tag{59}$$

Hence, the dynamics of system (1) in closed loop with the observer (16)–(21), the gradient estimator of surface (24) and the control law (29) is completely described by Eqs. (33)–(34), (45), (57), and (59), for which it is defined the state vector

$$\boldsymbol{y} \triangleq \left[\boldsymbol{x}_\mathrm{o}\ \boldsymbol{s}\ \Delta\bar{F}\ \tilde{\boldsymbol{J}}_{\varphi\mathrm{x}}^\mathrm{T}\right]^\mathrm{T}. \tag{60}$$

Now, the main result of this work is stated as follows.

Theorem 3.1. Consider the system dynamics (1) in closed loop with the observer (16)–(21) and the controller (29), for which the complete dynamics is given by Eqs. (33) and (34), (45), (57), and (59). Let y_max be a positive constant and let $\mathcal{D} \triangleq \{\boldsymbol{y} \in \mathbb{R}^{(p+2)n+4} \mid \|\boldsymbol{y}\| \leq y_\mathrm{max}\}$, where y_max is small

https://doi.org/10.1017/S0263574719000523 Published online by Cambridge University Press

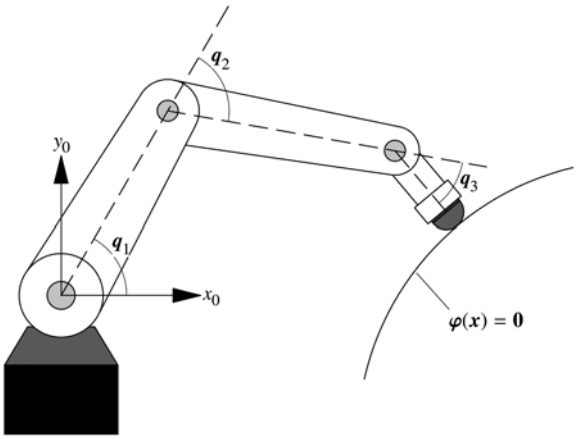

Fig. 2. Three link planar robot in contact with a curved surface.

enough for Fact 2.1 to hold. Assume that constraint (2) is smooth and that the manipulator tip never losses contact with the environment. Then a set of controller gains $\boldsymbol{K}_{\mathrm{p}}$, $\boldsymbol{K}_{\mathrm{v}}$, $\boldsymbol{K}_{\mathrm{i}}$, and k_{Fi} in Eq. (29), γ in Eq. (24), and a set of observer gains $\boldsymbol{\lambda}_0, \ldots, \boldsymbol{\lambda}_{p+1}$ in Eqs. (16)–(21) can always be found to achieve ultimate boundedness of the state $\boldsymbol{y}$ in Eq. (60) if the initial condition $\boldsymbol{y}(t_0)$ is chosen to satisfy (A51). Furthermore, the tracking errors $\boldsymbol{e}_1$, $\dot{\boldsymbol{e}}_1$, $\Delta\lambda$, and ΔF and the estimation errors $\boldsymbol{x}_{\mathrm{o}}$ and $\tilde{\boldsymbol{J}}_{\varphi \mathrm{x}}$ can be made arbitrarily small. △

Proof. See Appendix A. □

Remark 3.4. The gains for the observer (16)–(21), the surface estimator (24), the linear filter (27), and the hybrid force/motion controller (29) should be tuned as follows:

1. The poles of the observer (16)–(21) should be chosen as far in the left of the complex plane as allowed by the system bandwidth. For carrying out this tuning, any open-loop motion controller can be employed until the observation error $\tilde{\boldsymbol{q}}_1$ is as small as possible. These gains should be gradually incremented while the observation error does not present neither considerable peaking at the start of the transient response nor sensitivity to measurement noise.
2. The motion part of the force/position controller can be tuned as a common PID in free movement by forcing $\hat{\boldsymbol{Q}}_{\mathrm{x}} \equiv \boldsymbol{I}$ and making $\lambda_{\mathrm{d}} = k_{\mathrm{Fi}} = 0$ in Eq. (29).
3. The gain k_{Fi} can be adjusted by considering a motion/force controller with some known $\hat{\boldsymbol{Q}}_{\mathrm{x}}$, for example, a flat surface.
4. The surface estimator gain γ in Eq. (24) should be tuned carefully as it depends on the velocity of the task and on the surface curvature. If this gain is too low, the tip of the robot will may not be able to follow the surface contour. On the other hand, if this gain is too high, surface imperfections and measurement noise can lead to a wrong estimation and thus to a bad control performance.
5. Since Eq. (27) approximates a pure delay of one sampling period, η can be chosen simply as the inverse of the controller-loop sample time, that is, $\eta = 1/T$. □

4. Simulation and Experimental Results

In this section, both a numerical simulation and an experiment are presented to validate the proposed algorithm. The simulation is kept to show the good performance of the method in an ideal scenario. The experimental results, on the other hand, show the pertinence of the assumptions and the effectiveness of the approach even if there are unmodeled dynamics.

4.1. Numerical simulation

A three-link planar robot with revolute joints in contact with a curved rigid surface was considered, as depicted in Fig. 2. The parameters were taken from ref. [36] and correspond to the industrial robot *CRS A465*, where only joints 2, 3, and 5 are used to obtain a planar movement.

https://doi.org/10.1017/S0263574719000523 Published online by Cambridge University Press

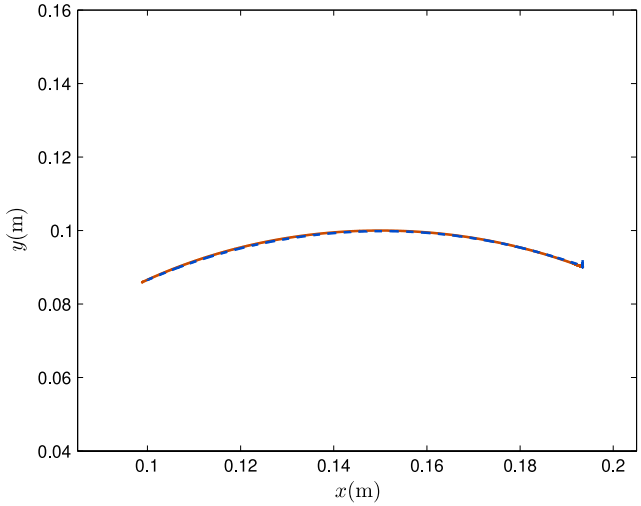

Fig. 3. Simulation: position tracking in the xy plane, real (—) and desired (- - -).

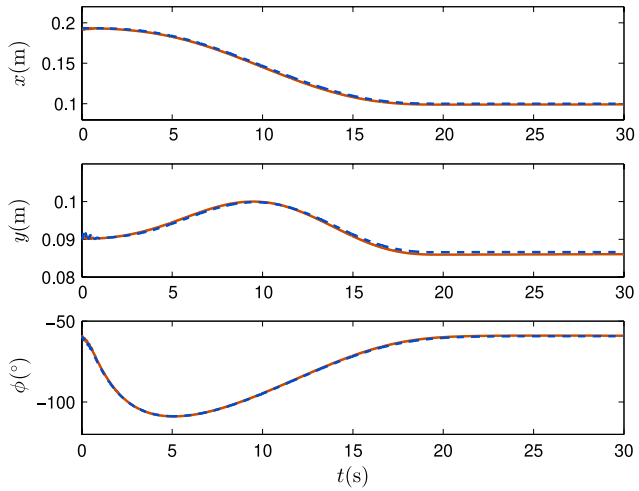

Fig. 4. Simulation: position tracking, real (——) and desired (- - -).

The task consisted on a trajectory over a curved surface in the plane given by the circle equation:

$$(x-h)^2+(y-k)^2=r^2, \tag{61}$$

where x, y are the Cartesian coordinates of the manipulator tip with respect to the base, $(h, k) = (0.15, 0)$ m are the coordinates of the center of the circle, and $r = 0.1$ m is the corresponding radius. The initial point is $(x, y) = (0.1934, 0.09)$ m from where a trajectory for the x coordinate was designed using a fifth-order polynomial to achieve the final point $x = 0.1$ m in a time of $t_f = 20$ s. The y coordinate was calculated online using (28). Also, the initial error between the actual and the estimated orientation was set to 30°.

The controller gains are $\boldsymbol{K}_p = \text{diag}\{4000, 4000, 200\}$, $\boldsymbol{K}_v = \text{diag}\{100, 100, 10\}$, $\boldsymbol{K}_i = \text{diag}\{100, 100, 100\}$, and $k_{Fi} = 2$. The surface estimation gain is $\gamma = 0.6$. The degree of the Taylor polynomial in Eq. (11) is $p = 2$. The poles of the observer are set to $p_1 = p_2 = p_3 = p_4 = -50$, resulting in the observer gains $\boldsymbol{\lambda}_0 = 6250000\boldsymbol{I}$, $\boldsymbol{\lambda}_1 = 500000\boldsymbol{I}$, $\boldsymbol{\lambda}_2 = 15000\boldsymbol{I}$, and $\boldsymbol{\lambda}_3 = 200\boldsymbol{I}$, where $\boldsymbol{I}$ is the identity matrix of $n \times n$. The constants ϵ in Eq. (24) and η in Eq. (27) have been chosen as $\epsilon = 0.0001$ and $\eta = 500$.

The trajectory in the xy plane is shown in Fig. 3 , while the position tracking for the x and y coordinates and the orientation angle ϕ are shown in Fig. 4. The corresponding tracking errors are displayed in Fig. 5.

https://doi.org/10.1017/S0263574719000523 Published online by Cambridge University Press

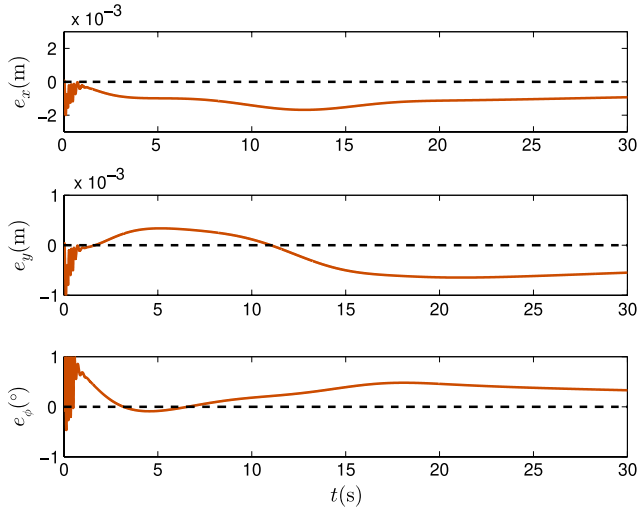

Fig. 5. Simulation: position tracking errors.

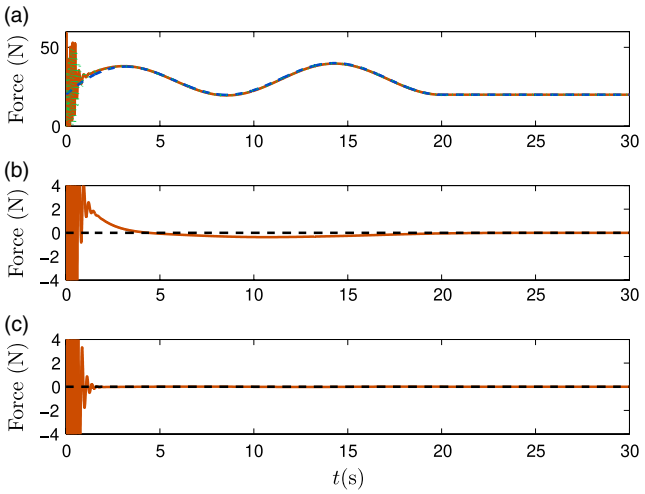

Fig. 6. Simulation: (a) force tracking (normal component), real (—), desired (- - -), and estimated (. . .), (b) force tracking error, and (c) force estimation error.

In Fig. 6 the desired, real and estimated forces are shown as well as the force tracking and force estimation errors. It can be seen that the force tracking and estimation are pretty accurate after the transient response. Finally, in Fig. 7 the estimation of the components of $\boldsymbol{J}_{\varphi \mathrm{x}}$ is displayed. It can be appreciated that the estimated components are maintained close to the real ones during the motion of the robot and converge to them in steady state.

4.2. Experimental validation

The experimental setup consists of a *Geomagic Touch* 3 degrees of freedom manipulator and a planar rigid surface as shown in Fig. 8. The sample time was $T = 0.002$s. The controller gains were $\boldsymbol{K}_{\mathrm{p}} = \mathrm{diag}\{2, 2, 2\}$, $\boldsymbol{K}_{\mathrm{v}} = \mathrm{diag}\{0.004, 0.004, 0.004\}$, $\boldsymbol{K}_{\mathrm{i}} = \mathrm{diag}\{0.25, 0.25, 0.25\}$, and $k_{\mathrm{Fi}} = 2$. The surface estimation gain was $\gamma = 0.02$. The degree of the Taylor polynomial in Eq. (11) is $p = 2$. The poles of the observer are set to $p_1 = p_2 = p_3 = p_4 = -120$, resulting in the observer gains $\boldsymbol{\lambda}_0 = 207360000\boldsymbol{I}$, $\boldsymbol{\lambda}_1 = 6912000\boldsymbol{I}$, $\boldsymbol{\lambda}_2 = 86400\boldsymbol{I}$, and $\boldsymbol{\lambda}_3 = 480\boldsymbol{I}$, where $\boldsymbol{I}$ is the identity matrix of $n \times n$. The constants ϵ in Eq. (24) and η in Eq. (27) have been chosen as $\epsilon = 0.0001$ and $\eta = 500$.

The experiment consisted in drawing a circle over a horizontal flat surface, while simultaneously applying a predefined time–dependent desired force over the surface. The desired x and y coordinates were planned offline by means of a fifth degree polynomial in time, while the z

https://doi.org/10.1017/S0263574719000523 Published online by Cambridge University Press

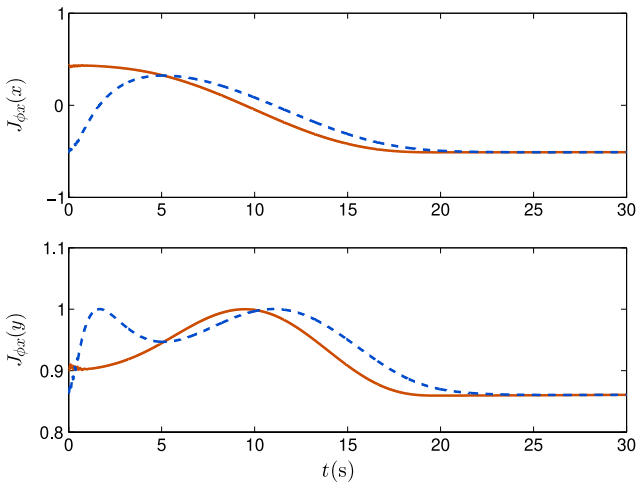

Fig. 7. Simulation: estimation of $\boldsymbol{J}_{\varphi x}$, real (—) and estimated (- - -).

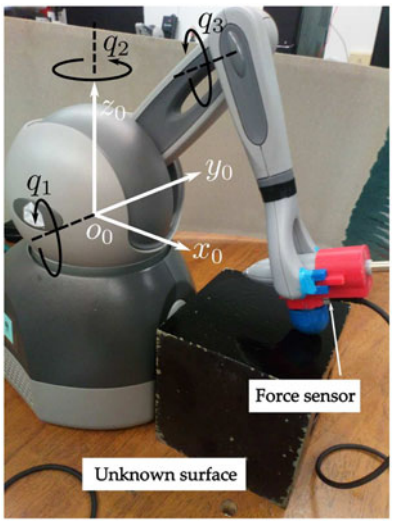

Fig. 8. Experimental setup.

coordinate was planned online to fulfill (28). The initial condition proposed for the gradient was $\hat{\boldsymbol{J}}_{\varphi x}(t_0) = \left[\sqrt{0.1}\ -\sqrt{0.1}\ \sqrt{0.8}\right]$. It is considered that the real gradient is $\boldsymbol{J}_{\varphi x}(t) = \left[0\ 0\ 1\right]$.

A projection of the trajectory in the xy plane is shown in Fig. 9. The position tracking in Cartesian coordinates is displayed in Fig. 10, while the corresponding tracking errors are shown in Fig. 11. Note that all the errors remain bounded and that the ultimate bound for these errors is close to zero.

In Fig. 12, the normal component of the desired, measured, and estimated contact forces is shown, as well as the corresponding force tracking error and force estimation error. Note that the errors remain bounded during all the experiments and are close to zero in steady state.

The evolution of the estimated gradient components is shown in Fig. 13 along with the expected values. Moreover, the (unitary) estimated gradient vector at some fixed times is displayed in Fig. 14. Although the estimated vector does never coincide exactly with the expected one, mainly due to the effect of the unmodeled dynamics, it evolves to a better estimation than the proposed initial condition.

4.3. Discussion

As it can be seen in the last two sections, the experimental results are not longer as accurate in performance as the simulation results. The main causes of this performance losing are the uncertainties in the mathematical model and the external disturbances. Notice that any external disturbance enters in the model (1) in the same manner as the contact forces vector. Since the observer (16)–(21) relies on

https://doi.org/10.1017/S0263574719000523 Published online by Cambridge University Press

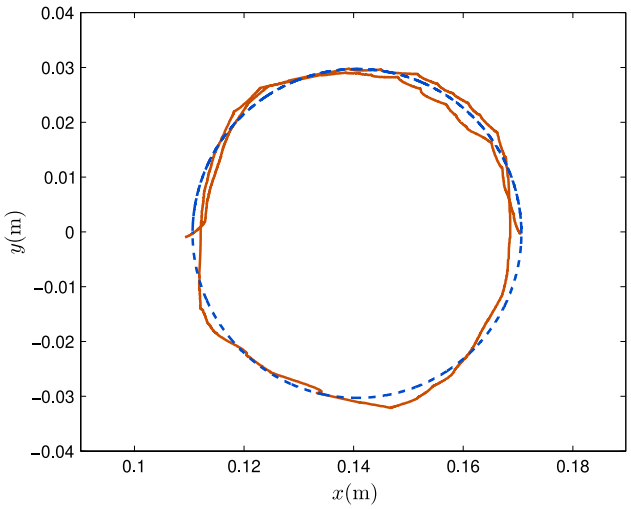

Fig. 9. Experiment: position tracking in the xy plane, real (—) and desired (- - -).

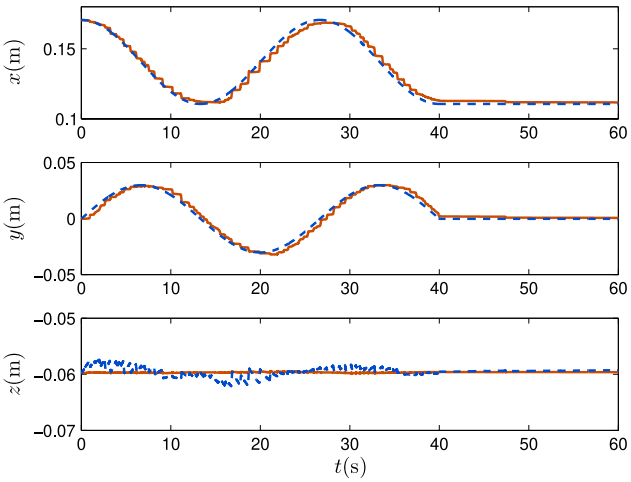

Fig. 10. Experiment: position tracking time evolution, real (—) and desired (- - -).

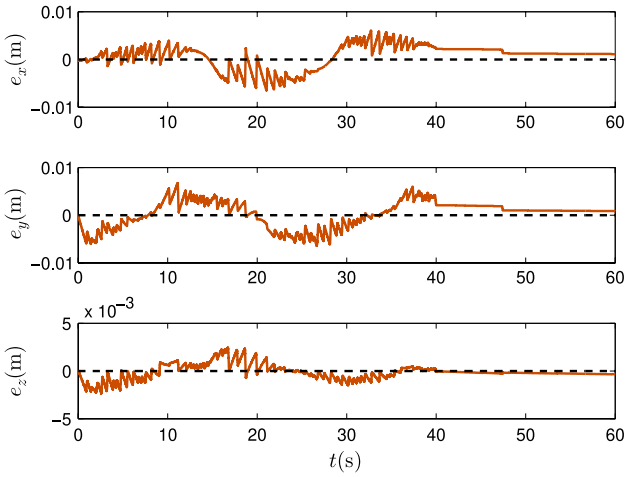

Fig. 11. Experiment: position tracking errors.

https://doi.org/10.1017/S0263574719000523 Published online by Cambridge University Press

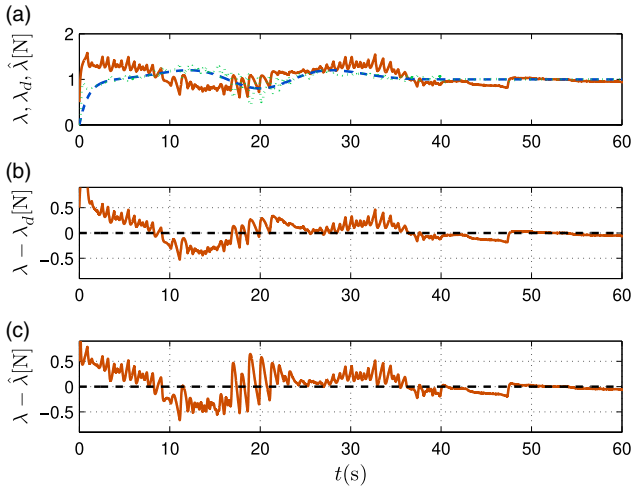

Fig. 12. Experiment: (a) force tracking (normal component), real (—), desired (- - -), and estimated (. . .), (b) force tracking error, and (c) force estimation error.

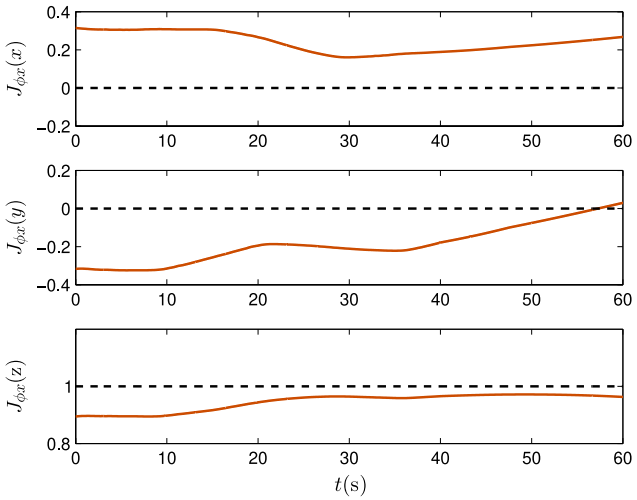

Fig. 13. Experiment: estimation of $\boldsymbol{J}_{\varphi \mathrm{x}}$, estimated (—) and actual (- - -).

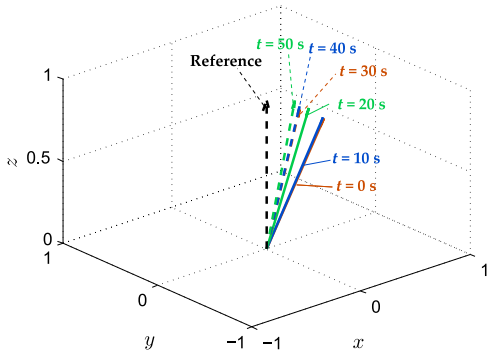

Fig. 14. Experiment: estimation of $\boldsymbol{J}_{\varphi \mathrm{x}}$ at different times.

the cancellation of all the manipulator dynamics terms, it can be seen that any external disturbance is undistinguishable from the contact force. On the other hand, the uncertainties on the Coriolis, damping, and gravity forces terms affect in the same way the force estimation as the external disturbances. Nevertheless, in this case, some of the well-known properties for robotic manipulators could

https://doi.org/10.1017/S0263574719000523 Published online by Cambridge University Press

be employed to eliminate or at least reduce the dependence on the accuracy of the model, which has not been done yet in the literature, to the best of the authors' knowledge. The inertia matrix uncertainties have also effect on the force estimation since this matrix is accounted in Eq. (23). The only difference is that the uncertainties enter in an homogeneous rather than in an additive form.

The same conclusions as above apply for the unknown surface estimator as it can be seen as the direction of the unknown force vector, while the contact force can be seen as the magnitude of the same vector.

5. Conclusions

In this work, under the assumption that neither the contact force nor the joint velocities are measurable, an extended state high-gain observer was designed to solve the problem of motion and force tracking over a geometrically uncertain surface. The proposed observer-based control scheme guarantees ultimate boundedness of position, velocity observation, and force tracking errors with an arbitrary small ultimate bound. Besides, the algorithm estimates online the normal vector to the surface to correct the desired position and orientation of the manipulator tip, which is equivalent to locally estimate the unknown contact surface while moving over it. The simulation results show that the proposed method is capable of accurately estimate the surface gradient, the joint velocity, and the contact force and at the same time while following a trajectory in position and force. On the other hand, in the experiment, the tracking and the estimation are no longer as accurate as in the simulations. This can be due to the presence of unmodeled dynamics, such as contact friction and disturbances. Nevertheless, all the tracking errors remained bounded with ultimate bound close to the origin of the error dynamics as guaranteed by the mathematical analysis.

As a future work, a model of contact friction will be included to improve the performance in the experimental results. Also, the application of the proposed force/velocity observer for the force control problem over deformable surfaces will be investigated.

Acknowledgments

This research is supported by the **DGAPA–UNAM** under Grant **IN114617**.

References

1. B. Siciliano and L. Villani, *Robot Force Control* (Kluwer Academic, New York, USA, 1999).
2. L. Zollo, B. Siciliano, C. Laschi, G. Teti and P. Dario, "An experimental study on compliance control for a redundant personal robot arm," *Robot. Auton. Syst.* **44**(2), 101–129 (2003).
3. L. Zollo, B. Siciliano, A. de Luca, E. Guglielmelli and P. Dario. "Compliance control for an anthropomorphic robot with elastic joints: Theory and experiments." *J. Dyn. Syst. Meas. Control*. **127**(3), 321–328 (2005).
4. T. Hanafusa and Q. Hunang, "Control of position, attitude, force and moment of 6-dof manipulator by impedance control." *Proceedings of the 15th International Conference on Control, Automation, Robotics and Vision (ICARCV)*, IEEE, Singapore (2018) pp. 274–279.
5. M. H. Raibert and J. J. Craig, "Hybrid position/force control of manipulators." *J. Dyn. Syst. Meas. Control*. **103**(2), 126–133 (1981).
6. S. Chiaverini and L. Sciavicco, "The parallel approach to force/position control of robotic manipulators," *IEEE Trans. Robot. Automat.* **9**(4), 361–373 (1993).
7. G. G. Muscolo, K. Hashimoto, A. Takanishi and P. Dario, "A comparison between two force-position controllers with gravity compensation simulated on a humanoid arm," *J. Robot.* **2013** (2013).
8. C. C. Cheah, S. P. Hou, Y. Zhao and J.-J. E. Slotine, "Adaptive vision and force tracking control for robots with constraint uncertainity," *IEEE/ASME Trans. Mechatron.* **15**(3), 389–397 (2010).
9. E. C. Dean-León, V. Parra-Vega and A. Espinosa-Romero, "Visual servoing for constrained planar robots subject to complex friction," *IEEE/ASME Trans. Mechatron.* **11**(4), 389–400 (2006).
10. A. C. Leite, F. Lizarralde and L. Hsu. "Hybrid adaptive vision/force control for robot manipulators interacting with unknown surfaces," *Int. J. Robot. Res.* **28**(7), 911–926 (2009).
11. V. Lippiello, B. Siciliano and L. Villani, "A position-based visual impedance control for robot manipulators." *Proceedings of the IEEE International Conference on Robotics and Automation (ICRA)*, IEEE, Rome, Italy (2007) pp. 2068–2073.
12. Y. H. Yin, Y. Xu, Z. H. Jiang and Q. R. Wang, "Tracking and understanding unknown surface with high speed by force sensing and control for robot." *IEEE Sensors J.* **12**(9), 2910–2916 (2012).
13. D. Wang, Y. C. Soh, Y. K. Ho and P. C. Müller, "Global stabilization for constrained robot motions with constraint uncertainties," *Robotica*. **16**(2), 171–179 (1998).
14. R. S. Jamisola, D. N. Oetomo, M. H. Ang, O. Khatib, T. M. Lim and S. Y. Lim. "Compliant motion using a mobile manipulator: an operational space formulation approach to aircraft canopy polishing", *Adv. Robot.* **19**(5), 613–634 (2005).

15. A. Jafari, R. Monfaredi, M. Rezaei, A. Talebi and S. S. Ghidary, "Sliding mode hybrid impedance control of robot manipulators interacting with unknown environments using VSMRC method," **In**: *Proceedings of the ASME 2012 International Mechanical Engineering Congress and Exposition*, Houston, TX, USA American Society of Mechanical Engineers (2012) pp. 1071–1081.
16. C. C. Cheah, S. Kawamura and S. Arimoto. "Stability of hybrid position and force control for robotic manipulator with kinematics and dynamics uncertainties," *Automatica*. **39**, 847–855 (2003).
17. C.-S. Chiu, K.-Y. Lian and T.-C. Wu. "Robust adaptive motion/force tracking control design for uncertain constrained robot manipulators," *Automatica*. **40**(12), 2111–2119 (2004).
18. Y. Karayiannidis and Z. Doulgeri, "Adaptive control of robot contact tasks with on-line learning of planar surfaces," *Automatica*. **45**(10), 2374–2382 (2009).
19. Y. Karayiannidis and Z. Doulgeri, "Robot contact tasks in the presence of control target distortions," *Robot. Auton. Syst.* **58**(5), 596–606 (2010).
20. M. Namvar and F. Aghili, "Adaptive force-motion control of coordinated robots interacting with geometrically unknown environments," *IEEE Trans. Robot.* **21**(4), 678–694 (2005).
21. J. Pliego-Jiménez and M. A. Arteaga-Pérez, "Adaptive position/force control for robot manipulators in contact with a rigid surface with uncertain parameters," *Eur. J. Control*. **22**, 1 – 12 (2015).
22. D. Wang and H. McClamroch, "Stability analysis of the equilibrium of a constrained mechanical system", *Int. J. Control*. **60**(5), 733–746 (1994).
23. Z. Doulgeri and Y. Karayiannidis, "Force/position regulation for a robot in compliant contact using adaptive surface slope identification," *IEEE Trans. Automat. Control*. **53**(9), 2116–2122 (2008).
24. L. Chan, F. Naghdy and D. Stirling, "Extended active observer for force estimation and disturbance rejection of robotic manipulators," *Robot. Auton. Syst.* **61**(12), 1277–1287 (2013).
25. J. M. Daly and D. W. L. Wang, "Time-delayed output feedback bilateral teleoperation with force estimation for n–dof nonlinear manipulators," *IEEE Trans. Control Syst. Technol.* **22**(1), 299–306 (2014).
26. P. J. Hacksel and S. E. Salcudean, "Estimation of environment forces and rigid-body velocities using observers," *Proceedings of the IEEE International Conference on Robotics and Automation (ICRA)*, vol. 2, San Diego, CA (May 1994) pp. 931–936.
27. J. C. Martínez-Rosas, M. A. Arteaga-Pérez and A. Castillo-Sánchez, "Decentralized control of cooperative robots without velocity-force measurements," *Automatica* **42**, 329-336 (2006).
28. M. A. Arteaga-Pérez, J. C. Rivera-Duenas and A. Gutiérrez-Giles, "Velocity and force observers for the control of robot manipulators," *J. Dyn. Syst. Meas. Control*. **135**(6), 064502 (2013).
29. A. Gutiérrez-Giles and M. A. Arteaga-Pérez, "GPI based velocity/force observer design for robot manipulators," *ISA Trans.* **53**(4), 929–938 (2014).
30. A. De Luca and R. Mattone, "Sensorless robot collision detection and hybrid force/motion control," *Proceedings of the IEEE International Conference on Robotics and Automation (ICRA)*, IEEE, Barcelona, Spain (2005) pp. 999–1004.
31. H. Sira-Ramírez, M. Ramírez-Neria and A. Rodríguez-Ángeles, "On the linear control of nonlinear mechanical systems," *Proceedings of the 49th IEEE Conference on Decision and Control*, IEEE, Atlanta, GA, USA (December 15–17, 2010).
32. V. Parra-Vega, A. Rodríguez-Angeles, S. Arimoto and G. Hirzinger, "High precision constrained grasping with cooperative adaptive handcontrol," *J. Intell. & Robot. Syst.* **32**, 235–254 (2001). 10.1023/A:1013987209547.
33. B. Siciliano, L. Sciavicco, L. Villani and G. Oriolo, *Robotics: Modelling, Planning and Control* (Springer-Verlag, London, UK, 2009).
34. J. C. Rivera-Dueñas and M. A. Arteaga-Pérez, "Robot force control without dynamic model: Theory and experiments," *Robotica* **31**, 149–171 (2013).
35. A. Wahrburg, E. Morara, G. Cesari, B. Matthias and H. Ding, "Cartesian contact force estimation for robotic manipulators using Kalman filters and the generalized momentum," *Proceedings of the IEEE International Conference on Automation Science and Engineering (CASE)*, IEEE, Gothenburg, Sweden (2015) pp. 1230–1235.
36. J. G. Lau and M. A. Arteaga, "Dynamic model and simulation of cooperative robots: A case study," *Robotica* **23**, 615–624 (2005).
37. R. M. Murray, Z. Li and S. S. Sastry, *A Mathematical Introduction to Robotic Manipulation* (CRC Press, Boca Raton, FL, 1994).
38. M. A. Arteaga-Pérez and A. Gutiérrez-Giles, "On the GPI approach with unknown inertia matrix in robot manipulators," *Int. J. Control*. **87**(4), 844–860 (2014).
39. H. K. Khalil, *Nonlinear Systems*, 3rd ed (Prentice–Hall, Upper Saddle River, NJ, 2002).

Appendix A. Proof of Theorem 3.1

As stated in Theorem 3.1, the stability result is local and valid only in a region $\mathcal{D}$ of interest, where it is assumed that Fact 2.1 holds. Therefore, it must be shown that any signal of interest is bounded whenever $\boldsymbol{y}_s \in \mathcal{D}$ and that, with a proper choice of gains, $\boldsymbol{y}_s$ will stay in $\mathcal{D}$ for all time and will tend to an arbitrary small region. Consider the next four steps:

https://doi.org/10.1017/S0263574719000523 Published online by Cambridge University Press

(a) First, we show that whenever the state $\boldsymbol{y}_s$ in Eq. (60) is bounded that is, $\boldsymbol{y} \in \mathcal{D}$, every signal of interest is also bounded. From Eq. (56), it is

$$\dot{\boldsymbol{\sigma}} = -\boldsymbol{K}_v^{-1}\bar{\boldsymbol{K}}_i \boldsymbol{Q}\boldsymbol{\sigma} + \boldsymbol{s}_p, \tag{A1}$$

where $\boldsymbol{s}_p$ is bounded in $\mathcal{D}$, because due to Fact 2.1, $\boldsymbol{s}_p$ and $\boldsymbol{s}_F$ are orthogonal. For the sake of simplicity, consider $\boldsymbol{K}_v = k_v \boldsymbol{I}$ and $\bar{\boldsymbol{K}}_i = \bar{k}_i \boldsymbol{I}$. Then it can be shown that $\boldsymbol{\sigma}$ and $\dot{\boldsymbol{\sigma}}$ are bounded and $\| \boldsymbol{Q}\boldsymbol{\sigma} \|$ and $\|\dot{\boldsymbol{\sigma}}\|$ can be made arbitrarily small by setting $\bar{k}_i$ large enough (see ref. [29] for details). As a result, from Eq. (50), $\dot{\boldsymbol{e}}_1$, $\boldsymbol{e}_1$, and $\int_0^t \boldsymbol{e}_1 \, d\vartheta$ are bounded, and since $\dot{\boldsymbol{q}}_d$ and $\boldsymbol{q}_d$ are bounded as well. Furthermore, $\boldsymbol{q}_1$, $\boldsymbol{q}_2$, $\hat{\boldsymbol{q}}_1$, $\dot{\hat{\boldsymbol{q}}}_1$, and $\hat{\boldsymbol{q}}_2$ are also bounded after Eq. (35) and because $\boldsymbol{x}_o$ is bounded in $\mathcal{D}$. From Eqs. (25) and (30)–(32), it follows that $\hat{\boldsymbol{J}}_{\varphi x}$, $\hat{\boldsymbol{J}}_\varphi$, $\hat{\boldsymbol{Q}}_x$, and $\hat{\boldsymbol{Q}}$ are bounded. This implies after Eq. (29) that $\boldsymbol{\tau}$ is bounded. Now, consider[37]

$$\begin{aligned}\boldsymbol{\lambda} = &\left(\boldsymbol{J}_\varphi(\boldsymbol{q}_1)\boldsymbol{H}^{-1}(\boldsymbol{q}_1)\boldsymbol{J}_\varphi^T(\boldsymbol{q}_1)\right)^{-1}\left\{\boldsymbol{J}_\varphi(\boldsymbol{q}_1)\boldsymbol{H}^{-1}(\boldsymbol{q}_1)\left(\boldsymbol{\tau} - \boldsymbol{N}(\boldsymbol{q}_1, \boldsymbol{q}_2)\right)\right. \\ &\left. + \boldsymbol{J}_\varphi(\boldsymbol{q}_1, \boldsymbol{q}_2)\boldsymbol{q}_2\right\}.\end{aligned} \tag{A2}$$

After Property 2.1, $\boldsymbol{\lambda}$ is bounded, which in turn means that $\boldsymbol{z}_1$ in (10) is bounded too. By taking into account Assumption 2.1 and that the surface is smooth, the partial derivatives $\partial\varphi(\boldsymbol{q}_1)/\partial\boldsymbol{q}_1, \partial^2\varphi(\boldsymbol{q}_1)/\partial\boldsymbol{q}_1^2, \ldots, \partial^{p+1}\varphi(\boldsymbol{q}_1)/\partial\boldsymbol{q}_1^{p+1}$ are bounded. Therefore, $\dot{\boldsymbol{J}}_\varphi(\boldsymbol{q}_1) = \left(\partial \boldsymbol{J}_\varphi(\boldsymbol{q}_1)/\partial \boldsymbol{q}_1\right)\dot{\boldsymbol{q}}_1$ must be bounded as well as $\boldsymbol{f}(t)$ in (42) and $\dot{\boldsymbol{q}}_r$ in (55). From (41), one can conclude that $\tilde{\boldsymbol{z}}_1$ is bounded and, as a consequence, $\hat{\boldsymbol{z}}_1$ and $\hat{\lambda}$ in (23) and $\Delta\bar{\lambda}$ in (33) must be bounded. After (24), (32), and (59), $\dot{\hat{\boldsymbol{J}}}_\varphi$, $\dot{\tilde{\boldsymbol{J}}}_\varphi$, and $\dot{\hat{\boldsymbol{Q}}}$ are bounded as well.

Taking into account (A2) and the manipulator models (8) and (9), one can write the joint acceleration as a function of only $(\boldsymbol{q}_1, \boldsymbol{q}_2, \boldsymbol{\tau})$, that is,

$$\dot{\boldsymbol{q}}_2 = \ddot{\boldsymbol{q}}_1 = \boldsymbol{f}_q(\boldsymbol{q}_1, \dot{\boldsymbol{q}}_1, \boldsymbol{\tau}), \tag{A3}$$

which clearly shows that $\dot{\boldsymbol{q}}_2$ is bounded. Since $\ddot{\boldsymbol{q}}_d$ and $\dddot{\tilde{\boldsymbol{q}}}_1$ are bounded, $\ddot{\boldsymbol{e}}_1$, $\ddot{\hat{\boldsymbol{q}}}_1$, and after Eq. (35) $\dot{\hat{\boldsymbol{q}}}_2$ must be bounded as well. Now, by similar arguments, $\boldsymbol{\tau}$ in Eq. (29) can be written as a function of bounded variables, that is,

$$\boldsymbol{\tau} = \boldsymbol{f}_\tau\left(\dot{\boldsymbol{q}}_d, \int_0^t \boldsymbol{e}_1 \, d\vartheta, \boldsymbol{e}_1, \tilde{\boldsymbol{q}}_1, \dot{\tilde{\boldsymbol{q}}}_1, \hat{\boldsymbol{Q}}, \lambda_d, \Delta\bar{F}\right). \tag{A4}$$

Therefore, its time derivative must be a function of the form

$$\dot{\boldsymbol{\tau}} = \dot{\boldsymbol{f}}_\tau\left(\dot{\boldsymbol{q}}_d, \ddot{\boldsymbol{q}}_d, \int_0^t \boldsymbol{e}_1 \, d\vartheta, \boldsymbol{e}_1, \dot{\boldsymbol{e}}_1, \tilde{\boldsymbol{q}}_1, \dot{\tilde{\boldsymbol{q}}}_1, \ddot{\tilde{\boldsymbol{q}}}_1, \hat{\boldsymbol{Q}}, \dot{\hat{\boldsymbol{Q}}}, \lambda_d, \dot{\lambda}_d, \Delta\bar{F}, \Delta\bar{\lambda}\right), \tag{A5}$$

which is bounded since it depends on variables we have already proven to be bounded. The time derivative of $\dot{\boldsymbol{q}}_r$ is given by

$$\begin{aligned}\ddot{\boldsymbol{q}}_r = &\ddot{\boldsymbol{q}}_d - \boldsymbol{\Lambda}\dot{\boldsymbol{e}}_1 - \boldsymbol{K}_v^{-1}\bar{\boldsymbol{K}}_i\dot{\boldsymbol{Q}}\boldsymbol{\sigma} - \boldsymbol{K}_v^{-1}\bar{\boldsymbol{K}}_i\boldsymbol{Q}\dot{\boldsymbol{\sigma}} + \frac{1}{2}\boldsymbol{K}_v^{-1}\dot{\boldsymbol{J}}_\varphi^T\Delta\lambda \\ &+ \frac{1}{2}\boldsymbol{K}_v^{-1}\boldsymbol{J}_\varphi^T\frac{d}{dt}(\Delta\lambda) + \frac{1}{2}k_{Fi}\boldsymbol{K}_v^{-1}\dot{\boldsymbol{J}}_\varphi^+\Delta\bar{F} + \frac{1}{2}k_{Fi}\boldsymbol{K}_v^{-1}\boldsymbol{J}_\varphi^+\Delta\bar{\lambda},\end{aligned} \tag{A6}$$

which again turns out to be bounded since from (A2), $\frac{d}{dt}(\Delta\lambda)$ is a function only of $(\boldsymbol{q}_1, \dot{\boldsymbol{q}}_1, \ddot{\boldsymbol{q}}_1, \boldsymbol{\tau}, \dot{\boldsymbol{\tau}})$. Then, there must exist a positive constant c_a such that $\boldsymbol{y}_a$ in (58) fulfills $\|\boldsymbol{y}_a\| \le c_a$, whenever $\boldsymbol{y} \in \mathcal{D}$. As a direct consequence, $\dot{\boldsymbol{s}}$ in Eq. (57) is bounded. By differentiating Eq. (56), one obtains

$$\begin{aligned}\dot{\boldsymbol{s}} = &\ddot{\boldsymbol{\sigma}} + \boldsymbol{K}_v^{-1}\bar{\boldsymbol{K}}_i\dot{\boldsymbol{Q}}\boldsymbol{\sigma} + \boldsymbol{K}_v^{-1}\bar{\boldsymbol{K}}_i\boldsymbol{Q}\dot{\boldsymbol{\sigma}} - \frac{1}{2}\boldsymbol{K}_v^{-1}\dot{\boldsymbol{J}}_\varphi^T\Delta\lambda - \frac{1}{2}\boldsymbol{K}_v^{-1}\boldsymbol{J}_\varphi^T\frac{d}{dt}(\Delta\lambda) \\ &- \frac{1}{2}k_{Fi}\boldsymbol{K}_v^{-1}\dot{\boldsymbol{J}}_\varphi^+\Delta\bar{F} - \frac{1}{2}k_{Fi}\boldsymbol{K}_v^{-1}\boldsymbol{J}_\varphi^+\Delta\bar{\lambda},\end{aligned} \tag{A7}$$

so that $\ddot{\boldsymbol{\sigma}}$ must be bounded.

https://doi.org/10.1017/S0263574719000523 Published online by Cambridge University Press

At this point, an iterative argument is carried out. First, by computing the time derivative of Eq. (A3) it is

$$\boldsymbol{q}_1^{(3)} = \dot{\boldsymbol{f}}_{\mathrm{q}}\left(\boldsymbol{q}_1, \dot{\boldsymbol{q}}_1, \ddot{\boldsymbol{q}}_1, \boldsymbol{\tau}, \dot{\boldsymbol{\tau}}\right), \tag{A8}$$

which shows that $\boldsymbol{q}_1^{(3)}$, $\boldsymbol{e}_1^{(3)}$, and $\hat{\boldsymbol{q}}_1^{(3)}$ are bounded. Combining Eqs. (16) and (17), it can be written

$$\hat{\boldsymbol{z}}_1 = \boldsymbol{f}_{\hat{z}_1}\left(\boldsymbol{q}_1, \ddot{\tilde{\boldsymbol{q}}}_1, \tilde{\boldsymbol{q}}_1, \dot{\tilde{\boldsymbol{q}}}_1, \hat{\boldsymbol{q}}_2, \boldsymbol{\tau}\right). \tag{A9}$$

This implies that

$$\dot{\hat{\boldsymbol{z}}}_1 = \dot{\boldsymbol{f}}_{\hat{z}_1}\left(\boldsymbol{q}_1, \dot{\boldsymbol{q}}_1, \ddot{\tilde{\boldsymbol{q}}}_1, \hat{\boldsymbol{q}}_1^{(3)}, \tilde{\boldsymbol{q}}_1, \dot{\tilde{\boldsymbol{q}}}_1, \ddot{\tilde{\boldsymbol{q}}}_1, \hat{\boldsymbol{q}}_2, \dot{\hat{\boldsymbol{q}}}_2, \boldsymbol{\tau}, \dot{\boldsymbol{\tau}}\right) \tag{A10}$$

is bounded and so are $\dot{\hat{\lambda}}$ and $\frac{\mathrm{d}}{\mathrm{d}t}(\Delta\bar{\lambda})$ as a consequence. From Eq. (24), it is

$$\dot{\hat{\boldsymbol{J}}}_{\varphi \mathrm{x}} = \dot{\boldsymbol{f}}_{\hat{\mathrm{J}}_{\varphi \mathrm{x}}}\left(\boldsymbol{q}_1, \hat{\boldsymbol{z}}_1\right), \tag{A11}$$

where Eq. (23) has been taken into account. Then, after Eq. (30) it means

$$\dot{\hat{\boldsymbol{J}}}_{\varphi} = \dot{\boldsymbol{f}}_{\hat{\mathrm{J}}_{\varphi}}\left(\boldsymbol{q}_1, \dot{\boldsymbol{q}}_1, \hat{\boldsymbol{z}}_1\right), \tag{A12}$$

$$\ddot{\hat{\boldsymbol{J}}}_{\varphi} = \ddot{\boldsymbol{f}}_{\hat{\mathrm{J}}_{\varphi}}\left(\boldsymbol{q}_1, \dot{\boldsymbol{q}}_1, \ddot{\boldsymbol{q}}_1, \hat{\boldsymbol{z}}_1, \dot{\hat{\boldsymbol{z}}}_1\right), \tag{A13}$$

which implies that $\ddot{\hat{\boldsymbol{Q}}}$ is bounded. On the other hand,

$$\ddot{\boldsymbol{J}}_{\varphi} = \boldsymbol{f}_{\mathrm{J}_{\varphi}}\left(\boldsymbol{q}_1, \dot{\boldsymbol{q}}_1, \ddot{\boldsymbol{q}}_1\right) \tag{A14}$$

must be bounded from the assumptions on the smoothness of the surface and because $\dot{\boldsymbol{q}}_1$ and $\dot{\boldsymbol{q}}_2$ are bounded, which along with Eq. (A13) means that $\dddot{\tilde{\boldsymbol{J}}}_{\varphi}$ is bounded. Now, from Eq. (A5), it is

$$\begin{aligned}\ddot{\boldsymbol{\tau}} = \ddot{\boldsymbol{f}}_{\tau}\Bigg(&\dot{\boldsymbol{q}}_{\mathrm{d}}, \ldots, \boldsymbol{q}_{\mathrm{d}}^{(3)}, \int_0^t \boldsymbol{e}_1 \,\mathrm{d}\vartheta, \boldsymbol{e}_1, \ldots, \ddot{\boldsymbol{e}}_1, \tilde{\boldsymbol{q}}_1, \ldots, \tilde{\boldsymbol{q}}_1^{(3)},\\ &\hat{\boldsymbol{Q}}, \ldots, \ddot{\hat{\boldsymbol{Q}}}, \lambda_{\mathrm{d}}, \ldots, \ddot{\lambda}_{\mathrm{d}}, \times\Delta\bar{F}, \Delta\bar{\lambda}, \frac{\mathrm{d}}{\mathrm{d}t}(\Delta\bar{\lambda})\Bigg),\end{aligned} \tag{A15}$$

which is bounded from the same arguments as those in the previous discussion. By the definition of $\boldsymbol{f}$ in Eq. (42), it can be written

$$f = f\left(\boldsymbol{q}_1, \dot{\boldsymbol{q}}_1, \dot{\boldsymbol{q}}_{\mathrm{d}}, \tilde{\boldsymbol{q}}_1, \dot{\tilde{\boldsymbol{q}}}_1\right), \tag{A16}$$

$$\dot{f} = \dot{f}\left(\boldsymbol{q}_1, \dot{\boldsymbol{q}}_1, \ddot{\boldsymbol{q}}_1, \dot{\boldsymbol{q}}_{\mathrm{d}}, \ddot{\boldsymbol{q}}_{\mathrm{d}}, \tilde{\boldsymbol{q}}_1, \dot{\tilde{\boldsymbol{q}}}_1, \ddot{\tilde{\boldsymbol{q}}}_1\right). \tag{A17}$$

As a result, from Eq. (41), one can conclude that $\dot{\tilde{z}}_1$ is bounded, and so is $\dot{z}_1$. Following this procedure iteratively, it is obtained

$$\boldsymbol{q}_1^{(p+1)} = \boldsymbol{f}_{\mathrm{q}}^{(p-1)}\left(\boldsymbol{q}_1, \ldots, \boldsymbol{q}_1^{(p)}, \boldsymbol{\tau}, \ldots, \boldsymbol{\tau}^{(p-1)}\right), \tag{A18}$$

which means that $\boldsymbol{q}_1^{(p+1)}$ and $\hat{\boldsymbol{q}}_1^{(p+1)}$ (and all their previous derivatives) are bounded. From Eq. (A10), it follows

$$\begin{aligned}\hat{\boldsymbol{z}}_1^{(p-1)} = \boldsymbol{f}_{\hat{z}_1}^{(p-1)}\Big(&\boldsymbol{q}_1, \ldots, \boldsymbol{q}_1^{(p-1)}, \hat{\boldsymbol{q}}_1, \ldots, \hat{\boldsymbol{q}}_1^{(p+1)}, \tilde{\boldsymbol{q}}_1, \ldots, \tilde{\boldsymbol{q}}_1^{(p)},\\ &\dot{\hat{\boldsymbol{q}}}_2, \ldots \hat{\boldsymbol{q}}_2^{(p-1)}, \boldsymbol{\tau}, \ldots, \boldsymbol{\tau}^{(p-1)}\Big),\end{aligned} \tag{A19}$$

which must be bounded as well as all its previous time derivatives. It also implies that $\ddot{\hat{\lambda}}, \ldots, \hat{\lambda}^{(p-1)}$ and $\mathrm{d}^2(\Delta\bar{\lambda})/\mathrm{d}t^2, \ldots, \mathrm{d}^{p-1}(\Delta\bar{\lambda})/\mathrm{d}t^{p-1}$ are bounded. In the same manner, from

https://doi.org/10.1017/S0263574719000523 Published online by Cambridge University Press

Eq. (A13), it is

$$\hat{\boldsymbol{J}}_{\varphi}^{(p)} = \boldsymbol{f}_{\hat{\mathrm{J}}_{\varphi}}^{(p)}\left(\boldsymbol{q}_1, \ldots, \boldsymbol{q}_1^{(p)}, \hat{\boldsymbol{z}}_1, \ldots, \hat{\boldsymbol{z}}_1^{(p-1)}\right). \tag{A20}$$

Also, from Eq. (A15), it is obtained

$$\boldsymbol{\tau}^{(p)} = \boldsymbol{f}_{\tau}^{(p)}\left(\dot{\boldsymbol{q}}_{\mathrm{d}}, \ldots, \boldsymbol{q}_{\mathrm{d}}^{(p+1)}, \int_0^t \boldsymbol{e}_1 \, \mathrm{d}\vartheta, \boldsymbol{e}_1, \ldots, \boldsymbol{e}_1^{(p)}, \tilde{\boldsymbol{q}}_1, \ldots, \tilde{\boldsymbol{q}}_1^{(p+1)}, \hat{\boldsymbol{Q}}, \ldots, \hat{\boldsymbol{Q}}^{(p)}, \lambda_{\mathrm{d}}, \ldots, \lambda_{\mathrm{d}}^{(p)}, \Delta\bar{F}, \Delta\bar{\lambda}, \ldots, \mathrm{d}^{(p-1)}(\Delta\bar{\lambda})/\mathrm{d}t^{(p-1)}\right),$$

which is bounded, since it is a function of bounded signals. On the other hand, from Eq. (A17), it can be written:

$$\boldsymbol{f}^{(p)} = \boldsymbol{f}^{(p)}\left(\boldsymbol{q}_1, \ldots, \boldsymbol{q}_1^{(p+1)}, \dot{\boldsymbol{q}}_{\mathrm{d}}, \ldots, \boldsymbol{q}_{\mathrm{d}}^{(p+1)}, \tilde{\boldsymbol{q}}_1, \ldots, \tilde{\boldsymbol{q}}_1^{(p+1)}\right), \tag{A21}$$

which is bounded with all its previous derivatives bounded too. From Eq. (41), it is computed

$$\tilde{\boldsymbol{q}}_1^{(p+1)} + \boldsymbol{\lambda}_{p+1}\tilde{\boldsymbol{q}}_1^{(p)} + \boldsymbol{\lambda}_p\tilde{\boldsymbol{q}}_1^{(p-1)} = \tilde{\boldsymbol{z}}_1^{(p-1)} + \boldsymbol{f}^{(p-1)}, \tag{A22}$$

which implies that $(\tilde{\boldsymbol{z}}_1, \ldots, \tilde{\boldsymbol{z}}_1^{(p-1)})$ are bounded too. Also, from Eqs. (10) and (A2), it can be seen that

$$\boldsymbol{z}_1 = \boldsymbol{f}_{\mathrm{z}_1}(\boldsymbol{q}_1, \dot{\boldsymbol{q}}_1, \boldsymbol{\tau}), \tag{A23}$$

from where it can be stated that all its time derivatives up to

$$\boldsymbol{z}_1^{(p)} = \boldsymbol{f}_{\mathrm{z}_1}^{(p)}\left(\boldsymbol{q}_1, \ldots, \boldsymbol{q}_1^{(p+1)}, \boldsymbol{\tau}, \ldots, \boldsymbol{\tau}^{(p)}\right) \tag{A24}$$

must be bounded as well. From Eqs. (12) to (15), it can be concluded that $(\boldsymbol{z}_1, \boldsymbol{z}_2, \ldots, \boldsymbol{z}_p, \dot{\boldsymbol{z}}_1, \dot{\boldsymbol{z}}_2, \ldots, \dot{\boldsymbol{z}}_p)$ and $\boldsymbol{r}^{(p)}$ must be bounded, since $\boldsymbol{z}_p = \boldsymbol{z}_1^{(p)}$. Furthermore, from Eq. (21), one can see that $\dot{\hat{\boldsymbol{z}}}_p$ is bounded as well. Also, since $(\boldsymbol{z}_1, \ldots, \boldsymbol{z}_1^{(p-1)})$ are bounded, one can easily show that the estimated variables $(\boldsymbol{z}_2, \ldots, \boldsymbol{z}_p, \dot{\boldsymbol{z}}_2, \ldots, \dot{\boldsymbol{z}}_{p-1})$ must be bounded. Moreover, all the related errors must be bounded as well.

(b) The second step of the proof is completely analogous to that given in ref. [29] from which only the main points are recalled. Let

$$V_{\mathrm{a}} = \boldsymbol{x}_{\mathrm{o}}^{\mathrm{T}}\boldsymbol{P}_{\mathrm{o}}\boldsymbol{x}_{\mathrm{o}}, \tag{A25}$$

with $\boldsymbol{x}_{\mathrm{o}}$ defined in Eq. (46) and $\boldsymbol{P}_{\mathrm{o}} = \boldsymbol{P}_{\mathrm{o}}^{\mathrm{T}} > \boldsymbol{O}$ given as the solution of

$$\boldsymbol{A}^{\mathrm{T}}\boldsymbol{P}_{\mathrm{o}} + \boldsymbol{P}_{\mathrm{o}}\boldsymbol{A} = -\boldsymbol{Q}_{\mathrm{o}}, \tag{A26}$$

where $\boldsymbol{Q}_{\mathrm{o}}$ is a positive definite matrix and $\boldsymbol{A}$ is given by Eq. (47). Whenever $\boldsymbol{y} \in \mathcal{D}$, $\boldsymbol{r}_{\mathrm{f}}$ in Eq. (45) is bounded and there must exist a constant, say $r_{\max}$, such that $\sup_{t_0 \le \vartheta \le t} \|\boldsymbol{r}_{\mathrm{f}}(\vartheta)\| \le r_{\max}$. The time derivative of V_{a} fulfills

$$\dot{V}_{\mathrm{a}} \le -\|\boldsymbol{x}_{\mathrm{o}}\|\left(\lambda_{\min}(\boldsymbol{Q}_{\mathrm{o}})\|\boldsymbol{x}_{\mathrm{o}}\| - 2\lambda_{\max}(\boldsymbol{P}_{\mathrm{o}})\|\boldsymbol{B}\|r_{\max}\right). \tag{A27}$$

Then, it follows

$$\dot{V}_{\mathrm{a}} \le 0 \quad \text{if} \quad \|\boldsymbol{x}_{\mathrm{o}}(t)\| \ge \frac{2\lambda_{\max}(\boldsymbol{P}_{\mathrm{o}})}{\lambda_{\min}(\boldsymbol{Q}_{\mathrm{o}})}\|\boldsymbol{B}\|r_{\max}, \tag{A28}$$

where $\lambda_{\min}(\cdot)$ and $\lambda_{\max}(\cdot)$ denote the minimum and the maximum eigenvalues of their arguments, respectively. Also, since the system (45) is linear, by properly choosing the eigenvalues of $\boldsymbol{A}$, there must exist an ultimate bound for $\boldsymbol{x}_{\mathrm{o}}$ given by[38]

$$\|\boldsymbol{x}_{\mathrm{o}}(t)\| \le \frac{n(p+1)}{|\lambda_{\max}(\boldsymbol{A})|}\|\boldsymbol{B}\|r_{\max}, \quad \text{as} \quad t \to \infty. \tag{A29}$$

https://doi.org/10.1017/S0263574719000523 Published online by Cambridge University Press

Since $n(p+1)$ is fixed and $|\lambda_{\max}(\boldsymbol{A})|$ can be chosen arbitrarily large, the ultimate bound of $\boldsymbol{x}_{\mathrm{o}}$ can be made arbitrarily small. Besides, it can be proved that the ultimate bound of $\boldsymbol{x}_{\mathrm{o}}$ also fulfills[39]

$$\|\boldsymbol{x}_{\mathrm{o}}(t)\| \leq \frac{2\lambda_{\max}(\boldsymbol{P}_{\mathrm{o}})}{\lambda_{\min}(\boldsymbol{Q}_{\mathrm{o}})}\sqrt{\frac{\lambda_{\max}(\boldsymbol{P}_{\mathrm{o}})}{\lambda_{\min}(\boldsymbol{P}_{\mathrm{o}})}}\|\boldsymbol{B}\|r_{\max}, \tag{A30}$$

which means (c.f. (A29)) that the term $\lambda_{\max}(\boldsymbol{P}_{\mathrm{o}})/\lambda_{\min}(\boldsymbol{Q}_{\mathrm{o}})$ can be made arbitrarily small. Notice that the ultimate bound of $\|\boldsymbol{x}_{\mathrm{o}}\|$ in Eq. (A29) can be made arbitrarily small independently of the norm of the state $\boldsymbol{y}$ in Eq. (60), that is, it depends only on the choose of the eigenvalues of $\boldsymbol{A}$ in Eq. (47).

(c) Till now it has been shown that whenever $\boldsymbol{y} \in \mathcal{D}$, every signal of interest is bounded and furthermore, the observation errors can be made arbitrarily small. The next step is to show that whenever $\boldsymbol{y}(t_0)$ is small enough, then it can be enforced for $\boldsymbol{y}$ to remain in $\mathcal{D}$ and that actually $\|\boldsymbol{y}\|$ can be made arbitrarily small, that is, $\boldsymbol{y}$ is ultimately bounded with ultimate bound arbitrarily small (see Fig A1 of ref. [29] for details).
Let

$$V_{\mathrm{s}} = \frac{1}{2}\boldsymbol{s}^{\mathrm{T}}\boldsymbol{H}(\boldsymbol{q})\boldsymbol{s} + \frac{1}{4}\frac{k_{\mathrm{Fi}}}{k_{\mathrm{v}}}(\Delta\bar{F})^2 \tag{A31}$$

be a positive function of $\boldsymbol{s}$ and $\Delta\bar{F}$.
From Properties 2.1–2.3, it can be shown that the time derivative of Eqs. (A31) along (34) and (57) is given by

$$\begin{aligned}\dot{V}_{\mathrm{s}} &= -\boldsymbol{s}^{\mathrm{T}}\boldsymbol{K}_{\mathrm{vD}}\boldsymbol{s} + \boldsymbol{s}^{\mathrm{T}}\boldsymbol{y}_{\mathrm{a}} - \frac{1}{4}k_{\mathrm{v}}^{-1}(\Delta\lambda)^2\boldsymbol{J}_{\varphi}\boldsymbol{J}_{\varphi}^{\mathrm{T}} - \frac{1}{2}\frac{k_{\mathrm{Fi}}}{k_{\mathrm{v}}}\Delta\bar{F}(\boldsymbol{J}_{\varphi}^{+})^{\mathrm{T}}\boldsymbol{H}(\boldsymbol{q})\tilde{\boldsymbol{z}}_1 \\ &\quad - \frac{1}{4}\frac{k_{\mathrm{Fi}}^2}{k_{\mathrm{v}}}(\Delta\bar{F})^2(\boldsymbol{J}_{\varphi}\boldsymbol{J}_{\varphi}^{\mathrm{T}})^{-1} \\ &\leq -k_{\mathrm{v}}\|\boldsymbol{s}\|^2 + c_{\mathrm{a}}\|\boldsymbol{s}\| + \frac{1}{2}\frac{k_{\mathrm{Fi}}\lambda_{\mathrm{H}}c_{\varphi}^{+}}{k_{\mathrm{v}}}|\Delta\bar{F}|\|\tilde{\boldsymbol{z}}_1\| - \frac{1}{4}\frac{k_{\mathrm{Fi}}^2 c_{\varphi}^{-}}{k_{\mathrm{v}}}|\Delta\bar{F}|^2,\end{aligned} \tag{A32}$$

where $c_{\varphi}^{+} \triangleq \|\boldsymbol{J}_{\varphi}^{+}\|_{\max}$ and $c_{\varphi}^{-} \triangleq \inf_{\boldsymbol{q}\in\mathbb{R}^n}\left\{\boldsymbol{J}_{\varphi}(\boldsymbol{q})\boldsymbol{J}_{\varphi}^{\mathrm{T}}(\boldsymbol{q})\right\}^{-1}$. Note that, since $\boldsymbol{J}_{\varphi}(\boldsymbol{q})$ is full rank for every $\boldsymbol{q} \in \mathbb{R}^n$ and the Jacobian of the manipulator is nonsingular and upper bounded, it is $0 < c_{\varphi}^{\pm} < \infty$. On the other hand, define

$$V_{\varphi\mathrm{x}} = \frac{1}{2}\tilde{\boldsymbol{J}}_{\varphi\mathrm{x}}\tilde{\boldsymbol{J}}_{\varphi\mathrm{x}}^{\mathrm{T}}. \tag{A33}$$

Its time derivative is given by

$$\dot{V}_{\varphi\mathrm{x}} = \tilde{\boldsymbol{J}}_{\varphi\mathrm{x}}\dot{\tilde{\boldsymbol{J}}}_{\varphi\mathrm{x}}^{\mathrm{T}} = -\tilde{\boldsymbol{J}}_{\varphi\mathrm{x}}\dot{\hat{\boldsymbol{J}}}_{\varphi\mathrm{x}}^{\mathrm{T}} + \tilde{\boldsymbol{J}}_{\varphi\mathrm{x}}\dot{\boldsymbol{J}}_{\varphi\mathrm{x}}^{\mathrm{T}}. \tag{A34}$$

After Eqs. (22) and (24), and since $\tilde{\boldsymbol{z}}_1 = \boldsymbol{z}_1 - \hat{\boldsymbol{z}}_1$, one obtains

$$\dot{V}_{\varphi\mathrm{x}} = -\frac{\gamma}{\hat{\lambda}+\epsilon}\tilde{\boldsymbol{J}}_{\varphi\mathrm{x}}\hat{\boldsymbol{Q}}_{\mathrm{x}}\left(\boldsymbol{J}_{\varphi\mathrm{x}}^{\mathrm{T}}\lambda - \boldsymbol{J}^{-\mathrm{T}}(\boldsymbol{q}_1)\boldsymbol{H}(\boldsymbol{q}_1)\tilde{\boldsymbol{z}}_1\right) + \tilde{\boldsymbol{J}}_{\varphi\mathrm{x}}\dot{\boldsymbol{J}}_{\varphi\mathrm{x}}^{\mathrm{T}}. \tag{A35}$$

Hence, because $\hat{\boldsymbol{Q}}_{\mathrm{x}}\hat{\boldsymbol{J}}_{\varphi\mathrm{x}}^{\mathrm{T}} = \boldsymbol{O}$ and $\hat{\boldsymbol{Q}}_{\mathrm{x}}\hat{\boldsymbol{Q}}_{\mathrm{x}} = \hat{\boldsymbol{Q}}_{\mathrm{x}} = \hat{\boldsymbol{Q}}_{\mathrm{x}}^{\mathrm{T}}$, it is

$$\dot{V}_{\varphi\mathrm{x}} = -\frac{\gamma}{\hat{\lambda}+\epsilon}\left(\tilde{\boldsymbol{J}}_{\varphi\mathrm{x}}\hat{\boldsymbol{Q}}_{\mathrm{x}}^{\mathrm{T}}\hat{\boldsymbol{Q}}_{\mathrm{x}}\tilde{\boldsymbol{J}}_{\varphi\mathrm{x}}^{\mathrm{T}}\lambda - \tilde{\boldsymbol{J}}_{\varphi\mathrm{x}}\hat{\boldsymbol{Q}}_{\mathrm{x}}\boldsymbol{J}^{-\mathrm{T}}(\boldsymbol{q}_1)\boldsymbol{H}(\boldsymbol{q}_1)\tilde{\boldsymbol{z}}_1\right) + \tilde{\boldsymbol{J}}_{\varphi\mathrm{x}}\dot{\boldsymbol{J}}_{\varphi\mathrm{x}}^{\mathrm{T}}. \tag{A36}$$

Since $\boldsymbol{q}_1$ and $\dot{\boldsymbol{q}}_1$ are bounded in $\mathcal{D}$ and the surface is assumed to be smooth, there must exist a positive constant, say v_{x}, such that $\|\dot{\boldsymbol{J}}_{\varphi\mathrm{x}}\| \leq v_{\mathrm{x}} < \infty$. Also, consider a closed subset of the workspace of the manipulator centred at $\{\boldsymbol{x} \in \mathbb{R}^n | \tilde{\boldsymbol{J}}_{\varphi\mathrm{x}}(\boldsymbol{x}) = \boldsymbol{0}\}$ and defined by $\mathcal{S} = \{\boldsymbol{x} \in \mathbb{R}^n | \|\tilde{\boldsymbol{J}}_{\varphi\mathrm{x}}(\boldsymbol{x})\| \leq \sqrt{2}\}$, that is, the region of the workspace where the angle, say α, between the normal to the surface $\boldsymbol{J}_{\varphi\mathrm{x}}$ and its estimate $\hat{\boldsymbol{J}}_{\varphi\mathrm{x}}$ is at most 90°, or equivalently $0 \leq \alpha \leq \pi/2$ (see Fig. A1). Notice

https://doi.org/10.1017/S0263574719000523 Published online by Cambridge University Press

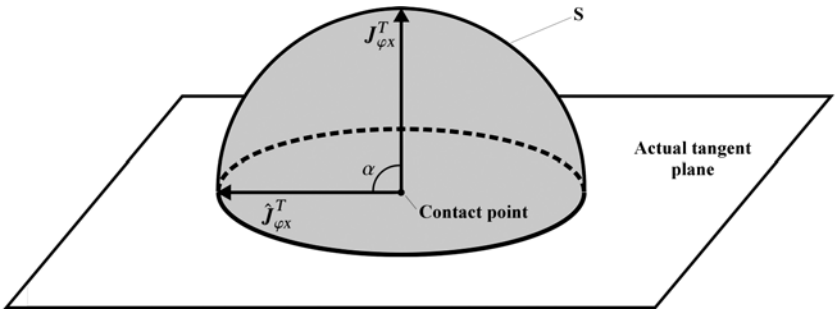

Fig. A1. Region $\mathcal{S}$.

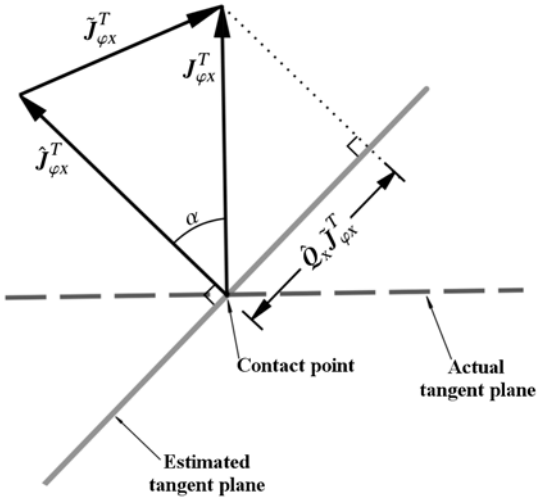

Fig. A2. Projections.

that this implies that the region $\mathcal{S}$ must be taken into account in the definition of the region $\mathcal{D}$. As can be seen in Fig. A2 (recalling that $\|\hat{\boldsymbol{J}}_{\varphi x}\| = \|\boldsymbol{J}_{\varphi x}\| = 1$), from the cosine rule one has (for $\alpha \leq \pi/2$)

$$\|\tilde{\boldsymbol{J}}_{\varphi x}\|^2 = 2\,(1 - \cos(\alpha)) \leq 2\left(1 - \cos^2(\alpha)\right) = 2\|\hat{\boldsymbol{Q}}_x \tilde{\boldsymbol{J}}_{\varphi x}^{\mathrm{T}}\|^2, \tag{A37}$$

since from the same figure, it can be seen that $\|\hat{\boldsymbol{Q}}_x \tilde{\boldsymbol{J}}_{\varphi x}^{\mathrm{T}}\| = \cos(\pi/2 - \alpha) = \sin(\alpha)$. Hence Eq. (A37) implies

$$\|\tilde{\boldsymbol{J}}_{\varphi x}\| \leq \sqrt{2}\|\hat{\boldsymbol{Q}}_x \tilde{\boldsymbol{J}}_{\varphi x}^{\mathrm{T}}\|. \tag{A38}$$

Moreover, given that the robot always exerts force over the surface, there must exist a constant, say c_λ, such that $\lambda \geq c_\lambda > 0$, $\forall t \geq t_0$. Also, since it has been proven that $\hat{\lambda}$ is bounded in $\mathcal{D}$, after (23) there must exist a constant, say $c_{\hat{\lambda}}$, such that $0 \leq \hat{\lambda} \leq c_{\hat{\lambda}} < \infty$, $\forall t \geq t_0$. Therefore, Eq. (A36) satisfies

$$\dot{V}_{\varphi x} \leq -\frac{\gamma c_\lambda}{\hat{\lambda} + \epsilon}\|\hat{\boldsymbol{Q}}_x \tilde{\boldsymbol{J}}_{\varphi x}^{\mathrm{T}}\|\left(\|\hat{\boldsymbol{Q}}_x \tilde{\boldsymbol{J}}_{\varphi x}^{\mathrm{T}}\| - \frac{\lambda_{\mathrm{H}}}{c_\lambda}\|\boldsymbol{J}^{-\mathrm{T}}(\boldsymbol{q}_1)\|\|\tilde{z}_1\| - \frac{c_{\hat{\lambda}} + \epsilon}{\gamma c_\lambda}\sqrt{2}v_x\right). \tag{A39}$$

By choosing the eigenvalues of $\boldsymbol{A}$ in Eq. (47) far away on the left in the complex plane, one guarantees that $(\tilde{\boldsymbol{q}}_1, \ldots, \tilde{\boldsymbol{q}}_1^{(p+2)})$ can be made arbitrarily small independently of the values of k_{v} and k_{Fi} (see Eq. (A29)). Notice that this implies after Eq. (42) that $\boldsymbol{f}(t)$, and hence $\tilde{z}_1$ in Eq. (41), can also be made arbitrarily small, which in turn implies that $(\lambda_{\mathrm{H}}/c_\lambda)\|\boldsymbol{J}^{-\mathrm{T}}(\boldsymbol{q}_1)\|\|\tilde{z}_1\|$ can

https://doi.org/10.1017/S0263574719000523 Published online by Cambridge University Press

be made arbitrarily small as well since after Assumption 2.1 $\boldsymbol{J}^{-1}(\boldsymbol{q}_1)$ always exists. Finally, the term $(c_{\hat{\lambda}} + \epsilon/\gamma c_\lambda)\sqrt{2}v_\mathrm{x}$ can be made arbitrarily small by setting γ sufficiently large. By defining

$$c_\mathrm{Q} \triangleq \frac{\lambda_\mathrm{H}}{c_\lambda}\|\boldsymbol{J}^{-\mathrm{T}}(\boldsymbol{q}_1)\|\|\tilde{\boldsymbol{z}}_1\| + \frac{c_{\hat{\lambda}} + \epsilon}{\gamma c_\lambda}\sqrt{2}v_\mathrm{x}, \tag{A40}$$

one has

$$\|\hat{\boldsymbol{Q}}_\mathrm{x}\tilde{\boldsymbol{J}}_{\varphi\mathrm{x}}^{\mathrm{T}}\| \geq c_\mathrm{Q} \implies \dot{V}_{\varphi\mathrm{x}} \leq 0. \tag{A41}$$

After Eq. (A33), it can be stated

$$\frac{1}{2}\|\tilde{\boldsymbol{J}}_{\varphi\mathrm{x}}\|^2 \leq V_{\varphi\mathrm{x}} \leq \frac{1}{2}\|\tilde{\boldsymbol{J}}_{\varphi\mathrm{x}}\|^2, \tag{A42}$$

which means that for $\dot{V}_{\varphi\mathrm{x}} \leq 0$

$$\|\tilde{\boldsymbol{J}}_{\varphi\mathrm{x}}(t)\| \leq \|\tilde{\boldsymbol{J}}_{\varphi\mathrm{x}}(t_0)\|, \quad \forall t \geq t_0. \tag{A43}$$

In the case $\|\hat{\boldsymbol{Q}}\tilde{\boldsymbol{J}}_{\varphi\mathrm{x}}(t)\| = \sqrt{2}c_\mathrm{Q}$, after (A38), the ultimate bound for $\|\tilde{\boldsymbol{J}}_{\varphi\mathrm{x}}\|$ is given by

$$\|\tilde{\boldsymbol{J}}_{\varphi\mathrm{x}}\| \leq \sqrt{2}c_\mathrm{Q}. \tag{A44}$$

Furthermore, the smaller $\|\hat{\boldsymbol{Q}}_\mathrm{x}\tilde{\boldsymbol{J}}_{\varphi\mathrm{x}}^{\mathrm{T}}\|$, the smaller $\|\tilde{\boldsymbol{J}}_{\varphi\mathrm{x}}\|$. By adding the functions defined in Eqs. (A25), (A31), and (A33), we obtain the positive definite function

$$\begin{aligned} V = V_\mathrm{a} + V_\mathrm{s} + V_{\varphi\mathrm{x}} &= \boldsymbol{x}_\mathrm{o}^{\mathrm{T}}\boldsymbol{P}_\mathrm{o}\boldsymbol{x}_\mathrm{o} + \frac{1}{2}\boldsymbol{s}^{\mathrm{T}}\boldsymbol{H}(\boldsymbol{q})\boldsymbol{s} + \frac{1}{4}\frac{k_\mathrm{Fi}}{k_\mathrm{v}}(\Delta\bar{F})^2 + \frac{1}{2}\tilde{\boldsymbol{J}}_{\varphi\mathrm{x}}\tilde{\boldsymbol{J}}_{\varphi\mathrm{x}}^{\mathrm{T}} \\ &= \boldsymbol{y}^{\mathrm{T}}\begin{bmatrix} \boldsymbol{P}_\mathrm{o} & \boldsymbol{O} & \boldsymbol{O} & \boldsymbol{O} \\ \boldsymbol{O} & \frac{1}{2}\boldsymbol{H}(\boldsymbol{q}) & \boldsymbol{O} & \boldsymbol{O} \\ \boldsymbol{O} & \boldsymbol{O} & \frac{1}{4}\frac{k_\mathrm{Fi}}{k_\mathrm{v}} & \boldsymbol{O} \\ \boldsymbol{O} & \boldsymbol{O} & \boldsymbol{O} & \frac{1}{2}\boldsymbol{I} \end{bmatrix}\boldsymbol{y} = \boldsymbol{y}^{\mathrm{T}}\boldsymbol{M}(\boldsymbol{q})\boldsymbol{y}, \end{aligned} \tag{A45}$$

where each $\boldsymbol{O}$ is a matrix or vector of zeros with appropriate dimensions. Given Property 2.1, we can find two positive constants, λ_m and λ_M, such that

$$\lambda_\mathrm{m}\|\boldsymbol{y}\|^2 \leq V(\boldsymbol{y}) \leq \lambda_\mathrm{M}\|\boldsymbol{y}\|^2. \tag{A46}$$

After Eqs. (A27), (A32), and (A39), the time derivative of Eq. (A45) along the trajectories of the system fulfills

$$\begin{aligned} \dot{V} \leq &-\lambda_{\min}(\boldsymbol{Q}_\mathrm{o})\|\boldsymbol{x}_\mathrm{o}\|\left(\|\boldsymbol{x}_\mathrm{o}\| - \frac{2\lambda_{\max}(\boldsymbol{P}_\mathrm{o})\|\boldsymbol{B}\|r_{\max}}{\lambda_{\min}(\boldsymbol{Q}_\mathrm{o})}\right) - k_\mathrm{v}\|\boldsymbol{s}\|\left(\|\boldsymbol{s}\| - \frac{c_\mathrm{a}}{k_\mathrm{v}}\right) \\ &- \frac{1}{4}\frac{k_\mathrm{Fi}^2 c_\varphi^-}{k_\mathrm{v}}|\Delta\bar{F}|\left(|\Delta\bar{F}| - \frac{2\lambda_\mathrm{H}c_\varphi^+}{k_\mathrm{Fi}c_\varphi^-}\|\tilde{\boldsymbol{z}}_1\|\right) \\ &- \frac{\gamma c_\lambda}{\hat{\lambda} + \epsilon}\|\hat{\boldsymbol{Q}}_\mathrm{x}\tilde{\boldsymbol{J}}_{\varphi\mathrm{x}}^{\mathrm{T}}\|\left(\|\hat{\boldsymbol{Q}}_\mathrm{x}\tilde{\boldsymbol{J}}_{\varphi\mathrm{x}}^{\mathrm{T}}\| - \frac{\lambda_\mathrm{H}}{c_\lambda}\|\boldsymbol{J}^{-\mathrm{T}}(\boldsymbol{q}_1)\|\|\tilde{\boldsymbol{z}}_1\| - \frac{c_{\hat{\lambda}} + \epsilon}{\gamma c_\lambda}\sqrt{2}v_\mathrm{x}\right). \end{aligned} \tag{A47}$$

According to the previous discussion, the terms

$$\frac{2\lambda_{\max}(\boldsymbol{P}_\mathrm{o})\|\boldsymbol{B}\|r_{\max}}{\lambda_{\min}(\boldsymbol{Q}_\mathrm{o})}, \ \frac{c_\mathrm{a}}{k_\mathrm{v}}, \ \frac{2\lambda_\mathrm{H}c_\varphi^+}{k_\mathrm{Fi}c_\varphi^-}\|\tilde{\boldsymbol{z}}_1\|, \ \frac{\lambda_\mathrm{H}}{c_\lambda}\|\boldsymbol{J}^{-\mathrm{T}}(\boldsymbol{q}_1)\|\|\tilde{\boldsymbol{z}}_1\|, \text{ and } \frac{c_{\hat{\lambda}} + \epsilon}{\gamma c_\lambda}\sqrt{2}v_\mathrm{x}$$

can be made arbitrarily small in $\mathcal{D}$ by choosing the eigenvalues of $\boldsymbol{A}$ in Eq. (47) far away on the left in the complex plane and the gains k_v, k_Fi, and γ large enough, as well as by choosing $y_{\max}$ small enough. Overall, we can always find a positive arbitrarily small constant μ such that

$$\dot{V} \leq 0 \quad \text{if} \quad \|\boldsymbol{y}\| \geq \mu. \tag{A48}$$

https://doi.org/10.1017/S0263574719000523 Published online by Cambridge University Press

Once $\|\boldsymbol{y}\| = \mu$, from Eq. (A46), the maximum value that $\|\boldsymbol{y}\|$ can take is given by

$$\lambda_{\mathrm{m}}\|\boldsymbol{y}\|^2 \leq V(\boldsymbol{y}) \leq \lambda_{\mathrm{M}}\mu^2 \implies \|\boldsymbol{y}\| \leq \sqrt{\frac{\lambda_{\mathrm{M}}}{\lambda_{\mathrm{m}}}}\mu \triangleq b, \tag{A49}$$

where b is the ultimate bound of the state $\boldsymbol{y}$. Recall that it must be guaranteed that $\|\boldsymbol{y}\| \leq y_{\max}$, $\forall t \geq t_0$. This can be done by setting gains large enough to satisfy

$$\mu < \sqrt{\frac{\lambda_{\mathrm{m}}}{\lambda_{\mathrm{M}}}}\, y_{\max}. \tag{A50}$$

Also, the initial condition must satisfy

$$\|\boldsymbol{y}(t_0)\| < \sqrt{\frac{\lambda_{\mathrm{m}}}{\lambda_{\mathrm{M}}}}\, y_{\max} \tag{A51}$$

to guarantee that $\boldsymbol{y}$ never leaves the region $\mathcal{D}$.

(d) Finally, since b can be made arbitrarily small, $\|\boldsymbol{y}\|$ can be made arbitrarily close to zero. This implies that observation errors $\tilde{\boldsymbol{q}}_1, \ldots, \tilde{\boldsymbol{q}}_1^{(p+2)}$ are made approximately zero. Therefore, after (35), $\tilde{\boldsymbol{q}}_2 \approx \boldsymbol{0} \implies \boldsymbol{q}_2 \approx \hat{\boldsymbol{q}}_2$, that is, $\hat{\boldsymbol{q}}_2$ is an arbitrarily close estimation of the vector of joint velocities $\boldsymbol{q}_2$. Also, we have proved that $\tilde{\boldsymbol{z}}_1 \approx \boldsymbol{0}$, which after (10) and (23) means that $\lambda - \hat{\lambda} \approx 0 \implies \hat{\lambda} \approx \lambda$ for $\lambda > 0$, which implies arbitrary close estimation of the contact force. Since the ultimate bound of $\|\boldsymbol{y}\|$, and therefore of $\|\boldsymbol{s}\|$ and $\|\Delta\bar{F}\|$, can be made arbitrarily small, from Eq. (56) one can see that the ultimate bound of $\Delta\lambda$ must be arbitrarily small as well, implying that force tracking is achieved.

https://doi.org/10.1017/S0263574719000523 Published online by Cambridge University Press